Kit (Thermo Scientific, Rockford, IL, USA), following the written instructions. Bovine serum albumin was used as a protein standard.

2.5. FD–LC–MS/MS method for liver mitochondrial proteomics analysis

The previous method was used for the FD procedure for liver mitochondrial proteins with DAABD-Cl [4], except for the amount of total protein; in brief, 60 μg of liver mitochondrial proteins was derivatized in 100 μL reaction mixture. Twenty microliters of the reaction mixture (12 μg proteins) was subjected to HPLC. Sample proteins amount per injection was low enough as compared to the maximum (24 μg) for separation on the non-porous column. The overall system consisted of a Hitachi L-2000 series HPLC system with a non-porous column (4.6 i.d. × 250 mm) at a column temperature of 60 °C [2] and a flow rate of 0.3 mL/min. Fluorescence detection was carried out at 505 nm (excitation at 395 nm). The compositions of the mobile phases were the same as described above. The 267.5 min gradient program was used to compare the non-porous column with the wide-pore column. The gradient elution was 16% B held over 5 min, to 25% in 10 min, to 43% B in 112.5 min, to 45% B in 135 min, to 55% B in 185 min, to 65% B in 215 min, and to 100% B in 267.5 min. The 535 min gradient program was used for proteomics analysis of mitochondrial proteins in livers of the hepatitis-infected mouse model. The gradient elution was 16% B held over 10 min, to 25% in 20 min, to 43% B in 225 min, to 45% B in 270 min, to 55% B in 370 min, to 65% B in 430 min, and to 100% B in 535 min. To keep the long life-time of the non-porous column, a washing operation was performed after operation of each analysis. The gradient time program of the washing operation was 100 to 0% B in 5 min and 0 to 100% B in 10 min at 0.3 mL/min of flow rate, which was repeated four times.

The isolated derivatized proteins were identified as reported in Ref. [5] using HPLC and tandem mass spectrometry. The obtained amino acids sequence data were searched for the taxonomy *Mus musculus* against the National Center for Biotechnology Information non-redundant (NCBInr) database using MASCOT version 2.1.03 (Matrix Science, Ltd., London, UK).

3. Result

3.1. Separation of DAABD-calcitonin in gradient elution with the non-porous column

The non-porous column was applied to separate fluorogenic derivatized calcitonin, a model peptide, to investigate its separation efficiency. Calcitonin (0.5 μM, M.W. 3418) was derivatized with a fluorogenic reagent, 7.0 mM DAABD-Cl, and subjected to HPLC-fluorescence detection in gradient elution on either the non-porous or the wide-pore column. Both columns were the same size (4.6 i.d. × 250 mm). The retention times and shapes of both DAABD-calcitonin peaks suggested that the non-porous column exhibited stronger affinity for the peptide and higher resolution than the wide-pore column (Fig. 2). The retention time of the compounds less retained on the non-porous column was shorter than that on the wide-pore column. The separation efficiencies of both columns were then compared utilizing the peak capacity, since the separation efficiency of HPLC columns in gradient elution is usually evaluated with column peak capacity P, while under isocratic conditions it is evaluated with theoretical plates N. The peak capacity represents the maximum theoretical number of components that can be separated in a column within a given gradient time. Each P value was then calculated from peak width w measured at 4σ

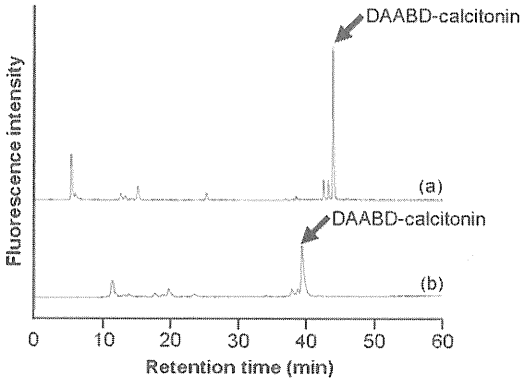

Fig. 2. Chromatograms obtained from DAABD-calcitonin separated in (a) the non-porous column or (b) the wide-pore column under gradient elution conditions. Chromatographic conditions are described in Section 2.

(13.4% of peak height) and the gradient time t_g according to Eq. (1) [12]:

$$P = 1 + \frac{t_g}{w} \quad (1)$$

The P value with the non-porous column was found to be three-fold higher than that with the wide-pore column under 60 min gradient conditions (197 with the non-porous column vs. 64 with the wide-pore column). In a similar experiment using a typical standard protein (β-lactoglobulin, M.W. 18,363), the P value exhibited the same tendency with both columns (data not shown). These results indicate that separation efficiency in the non-porous column was superior to that in the wide-pore column.

3.2. Optimized column length and flow rate with the non-porous column

In order to obtain appropriate separation efficiency, the gradient elution of DAABD-calcitonin was performed with different lengths (50, 100, 150, and 250 mm) of the non-porous column at different flow rates (0.2, 0.3, 0.4, and 0.5 mL/min). However, for the 250 mm-long column, the flow rate was limited to a maximum of 0.3 mL/min because of the durability of the HPLC flow (20 MPa) system used in the present experiment. DAABD-calcitonin was separated in the same 60 min gradient program as described in Section 3.1, and each P value was calculated according to Eq. (1). The P value increased with increasing column length and flow rate, indicating that separation efficiency was greater with a longer column and a higher flow rate (Fig. 3A). The same was true for β-lactoglobulin, a model protein (data not shown).

Moreover, mitochondrial protein extract was injected into each length of the columns at the maximum flow rate (0.3 or 0.5 mL/min) to investigate the separation of a real biological sample. The number of separated protein peaks increased with increasing column length: a 250 mm-long column at a 0.3 mL/min flow rate exhibited the highest separation efficiency for the actual protein mixture sample (Fig. 3B). Therefore, a column length of 250 mm with a flow rate of 0.3 mL/min was selected for separating the mitochondrial protein extract.

3.3. Comparison of the non-porous column with the wide-pore column for separating a mitochondrial protein extract

Based on the results above, the non-porous column (250 mm length with a flow rate of 0.3 mL/min) was applied to separate a mitochondrial protein extract. The chromatogram obtained under the appropriate conditions described in Section 2.5 was compared with that obtained from the wide-pore column (250 mm length,

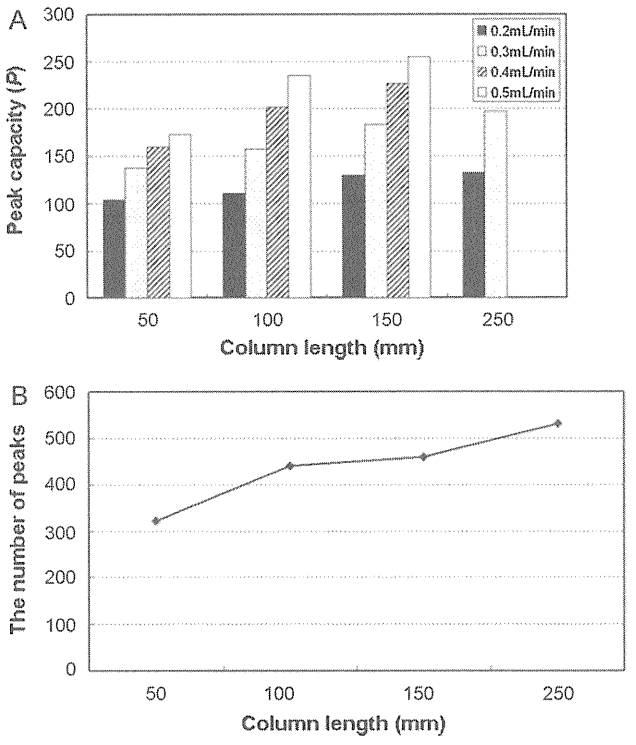

Fig. 3. (A) Peak capacities of the non-porous column with various column lengths (50, 100, 150, and 250 mm) at various flow rates (0.2, 0.3, 0.4, and 0.5 mL/min) in the gradient elution of DAABD-calcitonin. Each *P* value was calculated with Eq. (1) in Section 3.2. (B) The number of protein peaks separated in each length of the column (50, 100, 150, and 250 mm) obtained from the mitochondrial protein extract. The flow rate was 0.5 mL/min, except for the 250 mm column that had a 0.3 mL/min flow rate. The details are described in Section 2.

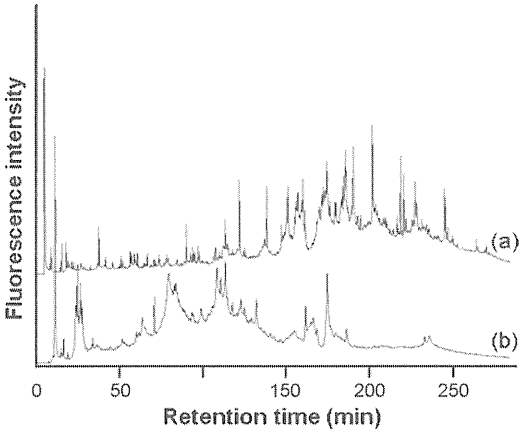

Fig. 4. Chromatograms of mouse liver mitochondrial proteins separated in (a) the non-porous column or (b) the wide-pore column. Chromatographic conditions are described in Section 2.

0.3 mL/min). Fig. 4a indicates that 420 protein peaks were obtained on the chromatogram with the non-porous column in 260 min analytical time. However, 160 protein peaks were not clearly separated in the chromatogram with the wide-pore column (Fig. 4b). This result clearly suggested that the non-porous column, rather than the wide-pore column, would be useful for proteomics analysis of mouse liver mitochondrial proteins with the FD–LC–MS/MS method.

Also, the retention times and peak shapes of the proteins injected into the non-porous column exhibited stronger adsorption and higher resolution than those injected into the wide-pore column. Furthermore, the retention time of the compounds less

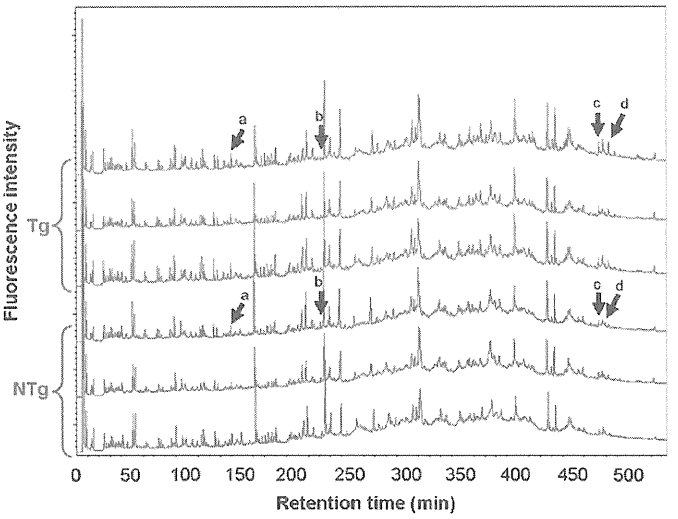

Fig. 5. Chromatograms of liver mitochondrial proteins in Tgs (red) and NTgs (blue) mice separated in the non-porous column. The peaks indicated by arrows fluctuated between Tgs and NTgs. Chromatographic conditions are described in Section 2. (For interpretation of the references to color in this figure legend, the reader is referred to the web version of the article.)

retained in the non-porous column was shorter than that on the wide-pore column.

3.4. Proteomics analysis of mitochondrial proteins in livers of hepatitis-infected mouse model

Differential proteomics analysis was performed on the non-porous column between mitochondrial protein samples extracted from livers of Tgs ($n = 3$) and NTgs ($n = 3$) mice aged 16 months. This age was selected based on the previous report that many proteins related to the function of mitochondrial events fluctuated in Tg. The appropriate separation conditions in HPLC afforded 500 protein peaks on each chromatogram for Tgs and NTgs in 9 h of analysis (Fig. 5), with each peak height representing the amount of each protein. The responsibility of this analysis was confirmed, based on the reproducibility of the retention times and the peak heights. The relative standard deviations (RSDs) of peaks a through d (Fig. 5) ranged from 0.0 to 0.5% for retention times and 0.4–18.0% for peak heights (for between-days, $n = 3$–6). The heights of peaks corresponding to specific retention times were compared between Tgs and NTgs. The expression of several peaks fluctuated, and each fluctuating peak fraction was collected, digested, and subjected to LC–MS/MS analysis to identify the protein. Table 1 summarizes the identified proteins. Three proteins were significantly up-regulated (Tg/NTg = 1.24–2.86, $0.05 \leq p < 0.10$) (Peaks a, c, and d in Fig. 5) in Tg, while one protein peak was significantly down-regulated (Tg/NTg = 0.44, $p < 0.05$) (Peak b in Fig. 5). Those four proteins were demonstrated for the first time in liver mitochondrial proteomics analysis.

4. Discussion

4.1. Comparison of the separation of DAABD-calcitonin and DAABD-β-lactoglobulin between the non-porous column and the wide-pore column

In order to determine the difference in separation between the non-porous column and the wide-pore column, a derivatized model peptide and protein (DAABD-calcitonin and DAABD-β-lactoglobulin) were separated. The retention times of the derivatized model samples were longer for the non-porous col-

Table 1
Differentially expressed liver mitochondrial proteins between Tgs and NTgs.

Peak number	Tg/NTg ratio		Protein name	Accession number	Score	Sequence coverage (%)
a	1.24	± 0.17	60S ribosomal protein L11	gi 13385408	129	12
b	0.44	± 0.33	Sterol-carrier protein 2	gi 45476581	278	10
c	1.51	± 0.35	NADH-cytochrome b5 reductase 3	gi 19745150	145	8
d	2.86	± 1.30	Hydroxysteroid (17-beta) dehydrogenase 13	gi 159573879	183	25

umn than for the wide-pore column. Since the surface of the non-porous column is covered with ODS (C18) and the surface of the wide-pore column consists of a less hydrophobic "reversed-phase" ligand than C18, stronger retention of the derivatized model samples should be caused by the hydrophobic interaction in the non-porous column. In contrast, considering the shortest retention times of the hydrophilic substances, the non-porous column should exhibit fewer void volumes than the wide-pore column. It was also shown that, considering the *P* (peak capacity) value for the non-porous column was threefold higher than that for the wide-pore column, the non-porous and small size (2 μm as compared to 3 μm of the wide-pore column) reduced eddy diffusion and mass-transfer resistance on separation and resulted in high-resolution chromatography [8]. This couldn't be caused by the narrow particle size distribution of the former column since the particle size distribution of both the columns were similar (D90/D10 < 1.4, and D90/D10 = 1.42 for the non-porous and the wide-pore, respectively, measured by laser diffraction particle size analysis and electrical sensing zone method).

4.2. Optimization of column length and flow rate for protein separation with the non-porous column

The effects of column length and flow rate on the *P* value were investigated using DAABD-calcitonin and DAABD-β-lactoglobulin to obtain optimal conditions for derivatized protein separation on the non-porous column. High *P* values were obtained using a longer column and a higher flow rate. This tendency agreed with the simulation of separation efficiency reported by Gilar et al. [12], indicating that the length of the non-porous column was proportional to separation efficiency. In this study, 0.3 mL/min was the maximum flow rate for the longest column (250 mm) because of the currently limited operating pressure (20 MPa). The LC system should be mechanically strong enough to withstand the ultrahigh pressures for further efficient separation in the non-porous Presto FF-C18 that might be 250 mm long and have a flow rate exceeding 0.3 mL/min. In this sense, in the future, further efficient separation should be examined utilizing an Ultra High Pressure Liquid Chromatography system. According to the results (Fig. 3A), the highest *P* value was obtained with a 150 mm length of column and a flow rate of 0.5 mL/min. However, more separated proteins were observed in the 250 mm-long column with a 0.3 mL/min flow rate for the mitochondrial sample (Fig. 3B). This is because the separable peaks from a large numbers of proteins in a real biological sample should be proportional to the column length. Another reason is that the dilution of the peak fraction in a 150 mm column with a high flow rate of 0.5 mL/min might be beyond the detection limit of the system. Therefore, a 250 mm column length with a flow rate of 0.3 mL/min was adopted as the optimal condition for separating liver mitochondrial proteins.

4.3. Application of the FD–LC–MS/MS method using the non-porous column for differential proteomics analysis of liver mitochondria

Nine hours of analysis indicated that the number (500) of mitochondrial protein peaks (Fig. 5) was similar to the number of extracted proteins from a whole cell separated with the wide-pore column (e.g., for mouse liver proteomics analysis) [4]. Concerning the life-time of the non-porous column, the life-time was long enough to analyze mitochondrial proteins about 40 times (400 h including the washing period) since the chromatogram obtained after 40 times analyses was the same as the initial one. That would be caused by the contribution of a washing operation after each analysis. This result suggests that the non-porous column could be substituted for the wide-pore column as a protein separation column for the FD–LC–MS/MS method.

Compared to the low reproducibility for the retention times of peaks in the previous report [9], the present differential proteomics analysis of liver mitochondria obtained reproducible retention times and peak heights (RSD less than 0.5% for retention times and less than 18.0% for peak heights). The reason for this superior reproducibility may be that in the FD–LC–MS/MS method, proteins were derivatized with the hydrophilic reagent and a low amount of proteins. These results indicate that the FD–LC–MS/MS method using the non-porous column can be used for differential proteomics analysis of liver mitochondria and results in identification of four fluctuating proteins between Tgs and NTgs.

4.4. Functions of the fluctuating liver mitochondrial proteins related to hepatocarcinogenesis

All the identified mitochondrial proteins in this study were demonstrated for the first time in liver proteomics analysis. Since mitochondria were extracted from mouse liver and analyzed for expression of proteins, it is assumed that the proteins inside the mitochondria were concentrated to a detectable level of each expression fluctuation.

Only one down-regulated peak in Tg was identified as sterol carrier protein 2 (SCP2), considering differences in localization between the deduced different types (SCP2 and SCPx) (reviewed in ref. [13]). SCP2 is related to intracellular lipid transport (e.g., cholesterol) from other intracellular membranes to mitochondria [14], as well as from the outer to the inner mitochondrial membrane for oxidation. Since lipids have accumulated in the hepatocytes of 16-month-old Tg mice, causing steatosis as previously reported [10], lipid transport to mitochondria might no longer be required. Thus, SCP2 was decreased in Tg through a negative feedback pathway. Also, SCP2 is reportedly involved in regulation of the signal pathway for lipids (reviewed in ref. [13]). These findings suggest that the decrease of SCP2 in Tg may suppress lipid transport to mitochondria, leading to inhibition of lipid signaling. In contrast, three proteins were demonstrated to be up-regulated in Tg. Hydroxysteroid (17-beta) dehydrogenase 13 (17βHSD13) is specifically expressed in liver [15]. It has been reported that the intracellular localization of 17βHSD13 is similar to that of HCV core protein in endoplasmic reticulum (ER), lipid droplets (LDs), and mitochondria [16–18], while it is unknown whether 17βHSD13 localizes in mitochondria or not. In general, 17βHSD family proteins catalyze the dehydrogenation reactions of the steroid skeleton with an excess of NADH or electrons. Although 17βHSD13 may play a key role in the next step of detoxification and/or utilization of lipid metabolites through the reaction, its specific substrate is not identified. At least, the increase of 17βHSD13 in Tgs would acti-

vate lipid metabolism. NADH-cytochrome b5 reductase 3 (CYB5R3) was observed in the plasma membrane, mitochondrial outer membrane, and ER. CYB5R3 in the mitochondrial electron-transfer system catalyzes the oxidation of NADH to NAD^+ (reviewed in Ref. [19]). For mitochondrial dysfunction, CYB5R3 is up-regulated due to an increase of the NADH/NAD^+ ratio, resulting in enhanced oxidation of NADH to NAD^+. Thus, an increase of CYB5R3 in Tg would accelerate aerobic respiration in mitochondria. In addition, 60S ribosomal protein L11 (RPL11) is associated with Mdm2, which is an E3 ligase for promoting p53 ubiquitination, resulting in prevention of the degradation of p53 [20,21]. The undegraded p53 in mitochondria reportedly causes apoptosis of cancer cells [22,23]. This finding suggests that up-regulated RPL11 would suppress the growth of hepatocarcinoma in transition out of hepatitis C. If hepatocarcinogenesis activates metabolism in Tg mice at the age of 16 months, 17βHSD13 and CYB5R3 might increase and accelerate lipid metabolism and aerobic respiration. Furthermore, a decrease of SCP2 might control lipid transport to mitochondria and thus maintain equilibrium through a negative feedback pathway. Considering these results, fluctuation of these proteins suggests that activation and suppression of hepatocarcinogenesis occur simultaneously in Tg mice at 16 months of age.

In conclusion, a novel non-porous column (Presto FF-C18) achieved good separation of liver mitochondrial proteins, which was hardly achieved on a wide-pore column such as Intrada WP-RP. Moreover, the FD–LC–MS/MS method with Presto FF-C18 demonstrated for the first time several fluctuating proteins performing differential proteomics analysis of liver mitochondrial proteins in a hepatitis-infected mouse model.

References

[1] H.J. Issaq, J. Blonder (Eds.), J. Chromatogr. B: Analyt. Technol. Biomed. Life Sci. Netherlands (2009) 1222.
[2] M. Masuda, H. Saimaru, N. Takamura, K. Imai, Biomed. Chromatogr. 19 (2005) 556.
[3] T. Ichibangase, H. Saimaru, N. Takamura, T. Kuwahara, A. Koyama, T. Iwatsubo, K. Imai, Biomed. Chromatogr. 22 (2008) 232.
[4] T. Ichibangase, K. Moriya, K. Koike, K. Imai, J. Proteome Res. 6 (2007) 2841.
[5] K. Imai, T. Ichibangase, R. Saitoh, Y. Hoshikawa, Biomed. Chromatogr. 22 (2008) 1304.
[6] H. Asamoto, T. Ichibangase, K. Uchikura, K. Imai, J. Chromatogr. A 1208 (2008) 147.
[7] T. Ichibangase, K. Imai, J. Proteome Res. 8 (2009) 2129.
[8] N. Wu, Y. Liu, M.L. Lee, J Chromatogr A, Netherlands (2006) 142.
[9] B.E. Chong, D.M. Lubman, F.R. Miller, A.J. Rosenspire, Rapid Commun. Mass Spectrom. 13 (1999) 1808.
[10] K. Moriya, H. Yotsuyanagi, Y. Shintani, H. Fujie, K. Ishibashi, Y. Matsuura, T. Miyamura, K. Koike, J. Gen. Virol. 78 (Pt 7) (1997) 1527.
[11] M.F. Lopez, B.S. Kristal, E. Chernokalskaya, A. Lazarev, A.I. Shestopalov, A. Bogdanova, M. Robinson, Electrophoresis 21 (2000) 3427.
[12] M. Gilar, A.E. Daly, M. Kele, U.D. Neue, J.C. Gebler, J. Chromatogr. A 1061 (2004) 183.
[13] F. Schroeder, B.P. Atshaves, A.L. McIntosh, A.M. Gallegos, S.M. Storey, R.D. Parr, J.R. Jefferson, J.M. Ball, A.B. Kier, Biochimica Et Biophysica Acta-Mol. Cell Biol. Lipids 1771 (2007) 700.
[14] G.G. Martin, H.A. Hostetler, A.L. McIntosh, S.E. Tichy, B.J. Williams, D.H. Russell, J.M. Berg, T.A. Spencer, J. Ball, A.B. Kier, F. Schroeder, Biochemistry 47 (2008) 5915.
[15] Y. Horiguchi, M. Araki, K. Motojima, Biochem. Biophys. Res. Commun. 370 (2008) 235.
[16] K. Moriya, H. Fujie, Y. Shintani, H. Yotsuyanagi, T. Tsutsumi, K. Ishibashi, Y. Matsuura, S. Kimura, T. Miyamura, K. Koike, Nat. Med. 4 (1998) 1065.
[17] R. Suzuki, S. Sakamoto, T. Tsutsumi, A. Rikimaru, K. Tanaka, T. Shimoike, K. Moriishi, T. Iwasaki, K. Mizumoto, Y. Matsuura, T. Miyamura, T. Suzuki, J. Virol. 79 (2005) 1271.
[18] B. Schwer, S.T. Ren, T. Pietschmann, J. Kartenbeck, K. Kaehlcke, R. Bartenschlager, T.S.B. Yen, M. Ott, J. Virol. 78 (2004) 7958.
[19] R. de Cabo, E. Siendones, R. Minor, P. Navas, Aging (Albany NY) 2 (2010) 63.
[20] K. Itahana, H. Mao, A.W. Jin, Y. Itahana, H.V. Clegg, M.S. Lindstrom, K.P. Bhat, V.L. Godfrey, G.I. Evan, Y.P. Zhang, Cancer Cell 12 (2007) 355.
[21] S. Fumagalli, A. Di Cara, A. Neb-Gulati, F. Natt, S. Schwemberger, J. Hall, G.F. Babcock, R. Bernardi, P.P. Pandolfi, G. Thomas, Nat. Cell Biol. 11 (2009) 501.
[22] N.D. Marchenko, A. Zaika, U.M. Moll, J. Biol. Chem. 275 (2000) 16202.
[23] M. Mihara, S. Erster, A. Zaika, O. Petrenko, T. Chittenden, P. Pancoska, U.M. Moll, Mol. Cell 11 (2003) 577.

JVI Journals.ASM.org

Establishment of a Novel Permissive Cell Line for the Propagation of Hepatitis C Virus by Expression of MicroRNA miR122

Hiroto Kambara,[a] Takasuke Fukuhara,[a] Mai Shiokawa,[a] Chikako Ono,[a] Yuri Ohara,[a] Wataru Kamitani,[b] and Yoshiharu Matsuura[a]

Department of Molecular Virology[a] and Global COE Program,[b] Research Institute for Microbial Diseases, Osaka University, Osaka, Japan

The robust cell culture systems for hepatitis C virus (HCV) are limited to those using cell culture-adapted clones (HCV in cell culture [HCVcc]) and cells derived from the human hepatoma cell line Huh7. However, accumulating data suggest that host factors, including innate immunity and gene polymorphisms, contribute to the variation in host response to HCV infection. Therefore, the existing *in vitro* systems for HCV propagation are not sufficient to elucidate the life cycle of HCV. A liver-specific microRNA, miR122, has been shown to participate in the efficient replication of HCV. In this study, we examined the possibility of establishing a new permissive cell line for HCV propagation by the expression of miR122. A high level of miR122 was expressed by a lentiviral vector placed into human liver cell lines at a level comparable to the endogenous level in Huh7 cells. Among the cell lines that we examined, Hep3B cells stably expressing miR122 (Hep3B/miR122) exhibited a significant enhancement of HCVcc propagation. Surprisingly, the levels of production of infectious particles in Hep3B/miR122 cells upon infection with HCVcc were comparable to those in Huh7 cells. Furthermore, a line of "cured" cells, established by elimination of HCV RNA from the Hep3B/miR122 replicon cells, exhibited an enhanced expression of miR122 and a continuous increase of infectious titers of HCVcc in every passage. The establishment of the new permissive cell line for HCVcc will have significant implications not only for basic HCV research but also for the development of new therapeutics.

Hepatitis C virus (HCV) infects over 170 million people worldwide and frequently leads to persistent infection, which in turn can lead to chronic hepatitis, cirrhosis, and hepatocellular carcinoma (34). HCV belongs to the *Flaviviridae* family and has a single-stranded positive RNA genome of approximately 9.6 kb. The genome of HCV is translated into a single polyprotein at the endoplasmic reticulum (ER) membrane and is then cleaved by host- and virus-encoded proteases, resulting in 10 structural and nonstructural proteins (41, 44). Due to the lack of a small-animal model and an efficient cell culture system, efforts to understand the HCV life cycle as well as development of anti-HCV drugs have been hampered (42). In a major breakthrough, HCV replicon cells, in which HCV RNA autonomously replicates, were established by Lohmann et al. (37). Afterwards, the infectious HCV in cell culture (HCVcc), based on the genotype 2a JFH1 strain in combination with the human hepatocellular carcinoma cell line Huh7, was developed (36, 64, 70). On the basis of the results obtained with these *in vitro* systems, the life cycle of HCV was clarified, and substantial progress has been made in screening host factors involved in HCV propagation as well as anti-HCV drug candidates (20, 51). Among them, a liver-specific microRNA (miRNA), miR122, has been shown to be one of the most important host factors for HCV replication.

miRNAs are small noncoding RNAs that consist of 20 to 25 nucleotides and modulate gene expression in plants and animals (3, 26). Most miRNAs negatively regulate translation through interaction with the 3′ untranslated region (UTR) of mRNA in a sequence-specific manner. Some of them have been shown to play important roles in the viral life cycle (56). Interestingly, miR122 has been shown to bind to HCV 5′ UTRs and to enhance translation and replication of HCV RNA (23, 28, 29, 38, 52). In addition, enhancement of HCVcc propagation through the direct interaction of miR122 with HCV 5′ UTR has been demonstrated (27). Recently, intravenous administration of the locked nucleic acid (LNA) complementary to miR122 was shown to suppress the propagation of HCV in chimpanzees chronically infected with HCV, suggesting that miR122 is a promising therapeutic target for chronic hepatitis C (31).

It has been shown that HCV exploits various host factors to form a replication complex for efficient replication (43). *In vitro* propagation of HCV is limited to Huh7 cells and their derivatives, and thus, it is important to confirm the data obtained in Huh7 cells by using other human liver cell lines, because the patterns of gene expression vary among cell lines. Although establishment of an HCV replicon system based on liver cell lines has been reported (11, 66), robust propagation of HCVcc in well-characterized human liver cell lines other than Huh7 cells has not succeeded yet. The gene expression profile of mice xenotransplanted with human hepatocytes from different donors inoculated with a single source of HCV revealed that host factors contributed to the variation in host response to HCV infection, including the activation of innate antiviral signaling pathways (65). Furthermore, gene polymorphism in interleukin 28B (IL-28B) was shown to be associated with natural clearance (62) and response to combination therapy with interferon (IFN) and ribavirin (19, 58, 59). Therefore, the solely available *in vitro* propagation system for HCVcc, employing Huh7-derived cells, is not sufficient. The establishment of alternative HCV strains and permissive cell lines is needed to elucidate molecular mechanisms of propagation and pathogenesis of HCV in more detail.

Although there have been several attempts to generate chime-

Received 18 September 2011 Accepted 11 November 2011
Published ahead of print 23 November 2011
Address correspondence to Yoshiharu Matsuura, matsuura@biken.osaka-u.ac.jp.
H. Kambara and T. Fukuhara contributed equally to this article.

doi:10.1128/JVI.06242-11

ric HCVs based on the JFH1 strain (21) and an infectious clone of genotype 1a, H77S, that produces fewer infectious particles than the genotype 2a JFH1 strain (68), propagation of HCV was still limited to Huh7 cells. Exogenous expression of miR122 has been shown to support HCV RNA replication in a human embryonic kidney epithelial cell line and mouse embryonic fibroblasts (7, 35), and we therefore thought that the possibility of complete propagation of HCVcc in various human liver cell lines by the expression of miR122 needed to be examined. Among the cell lines that we examined, Hep3B cells, which were established from human liver tumor biopsy samples in 1976 (1) and have been well characterized as model liver cells in various fields of research (47, 55, 63, 67), were shown to support the efficient propagation of HCVcc comparable to that in Huh7 cells by the expression of miR122. Establishment of novel cell culture systems through the exogenous expression of miR122 provides a clue to understanding the precise roles of miR122 in the life cycle of HCV.

MATERIALS AND METHODS

Plasmids. The cDNA clones of wild-type miR122 (WT-miR122), single mutant miR122 (sMT-miR122), double mutant miR122 (dMT-miR122), *Aequorea coerulescens* green fluorescent protein (AcGFP), and claudin-1 (CLDN) were inserted between the XhoI and XbaI sites of a lentiviral vector, pCSII-EF-RfA, which was kindly provided by M. Hijikata, and the resulting plasmids were designated pCSII-EF-WT-miR122, pCSII-EF-sMT-miR122, pCSII-EF-dMT-miR122, pCSII-EF-AcGFP, and pCSII-EF-Claudin1, respectively. pHH-JFH1 was kindly provided by T. Wakita (39). pHH-JFH1-E2p7NS2mt contains three adaptive mutations in pHH-JFH1 (53). pFGR-JFH1 and pSGR-JFH1 encoded a full-length and a subgenomic cDNA of the JFH1 strain, respectively. The complementary sequence of miR122 was inserted into the PmeI site of the pmirGLO vector (Promega, Madison, WI), and the resulting plasmid was designated pmirGLO-miR122comp. pIFNβ-Luc and pISRE-Luc carrying a firefly luciferase gene under the control of the beta IFN (IFN-β) and interferon-sensitive response element (ISRE) promoters, respectively, were kindly provided by T. Kawai and S. Akira. The internal control plasmid encoding a *Renilla* luciferase (pRL-TK) was purchased from Promega. The plasmids used in this study were confirmed by sequencing with an ABI Prism 3130 genetic analyzer (Applied Biosystems, Tokyo, Japan).

Cells. All cell lines were cultured at 37°C under the condition of a humidified atmosphere and 5% CO_2. The human embryonic kidney 293T cell line and hepatocellular carcinoma cell lines Huh7, Huh6/CLDN, HepG2/CD81, Hep3B, and PKC/PRL/5 were maintained in Dulbecco's modified Eagle's medium (DMEM; Sigma, St. Louis, MO) supplemented with 100 U/ml penicillin, 100 μg/ml streptomycin, and 10% fetal calf serum (FCS). HepG2/CD81 cells were generated as described previously (60). Huh6 cells were transduced with a lentiviral vector expressing claudin-1, and the resulting cells were designated Huh6/CLDN. The Huh7-derived cell line Huh7.5.1 was kindly provided by F. Chisari and was maintained in DMEM containing nonessential amino acids (NEAA), 100 U/ml penicillin, 100 μg/ml streptomycin, and 10% FCS. Hep3B replicon cells harboring the subgenomic HCV RNA were maintained in DMEM containing 10% FCS, NEAA, and 400 μg/ml G418 (Nakalai Tesque, Kyoto, Japan).

Viruses. pHH-JFH1-E2p7NS2mt was transfected into Huh7.5.1 cells, and the culture supernatants were collected after serial passages. The infectivity of HCVcc was determined by focus-forming assay and expressed in focus-forming units (FFU) (64). The lentiviral vectors and ViraPower lentiviral packaging mix (Invitrogen, San Diego, CA) were cotransfected into 293T cells, and the supernatants were recovered at 48 h posttransfection. The culture supernatants were centrifuged at 1,000 $\times$ *g* for 5 min and cleared through a 0.45-μm-pore-size filter. The lentivirus titer was determined by a Lenti-X quantitative reverse transcription (qRT)-PCR titration kit (Clontech, Mountain View, CA). The vesicular stomatitis virus (VSV) variant NCP12.1, derived from the Indiana strain, was kindly provided by M. Whitt. Pseudotype VSVs bearing the HCV E1 and E2 glycoproteins (HCVpv) and VSV G protein (VSVpv) were prepared as described previously (60). The infectivity of the pseudotype viruses was assessed by the expression of luciferase, determined by a Bright-Glo luciferase assay system (Promega) following a protocol provided by the manufacturer and expressed in relative light units (RLU).

Reagents and antibodies. Cyclosporine (CsA) and human recombinant IFN-α2 were purchased from Sigma and R&D Systems (Minneapolis, MN), respectively. BODIPY 558/568 lipid probe was purchased from Invitrogen. Poly(I·C) was purchased from InvivoGen (San Diego, CA). LNAs complementary to miR122 (LNA-miR122; 5′-CcAttGTcaCaCtCC-3′) and its negative control (LNA-Cont; 5′-CcAttCTgaCcCtAC-3′) (LNA in capital letters, DNA in lowercase letters; sulfur atoms in oligonucleotide phosphorothioates are substituted for nonbridging oxygen atoms; capital C indicates LNA methylcytosine) (14) were purchased from Gene Design (Osaka, Japan). miScript miRNA mimics hsa-miR122 and its negative control were purchased from Qiagen (Valencia, CA). Mouse monoclonal antibodies to HCV NS5A and β-actin were purchased from Austral Biologicals (San Ramon, CA) and Sigma, respectively. Mouse anti-apolipoprotein E (anti-ApoE), rabbit anti-diacylglycerol acyltransferase 1 (DGAT1), rabbit anti-signal transducer and activators of transcription 2 (anti-STAT2), and rabbit anti-IFN regulatory factor 3 (anti-IRF3) antibodies were purchased from Santa Cruz (Santa Cruz, CA). Rabbit anti-HCV core protein was prepared as described previously (45). Phycoerythrin (PE)-conjugated anti-human CD81 (anti-hCD81) and anti-mouse IgG antibodies were purchased from BD Biosciences (Franklin Lakes, NJ). Mouse anti-double-stranded RNA (anti-dsRNA) IgG2a (J1 and K2) antibodies were from Biocenter Ltd. (Szirak, Hungary). Alexa Fluor 488 (AF488)-conjugated anti-mouse and -rabbit IgG and AF594-conjugated anti-rabbit IgG antibodies were from Invitrogen.

Quantitative RT-PCR. For quantitation of HCV RNA, total RNA was prepared from cells by using an RNeasy minikit (Qiagen). The synthesis of a first-stranded cDNA and quantitative RT-PCR were performed using TaqMan EZ RT-PCR core reagents and an ABI Prism 7000 system (Applied Biosystems) according to the manufacturer's protocol. For quantitation of miRNA, total RNA was prepared from cells by using an miRNeasy minikit (Qiagen), and miR122 was estimated by using miR122-specific RT primers and amplified using specific primers provided in the TaqMan MicroRNA assays (Applied Biosystems) according to the manufacturer's protocol. U6 small nuclear RNA (snRNA) was used as an internal control. Fluorescent signals were analyzed by an ABI Prism 7000 system (Applied Biosystems).

Transfection and immunoblotting. Cells were transfected with the plasmids by using *Trans* IT LT-1 (Mirus, Madison, WI) or Lipofectamine 2000 (Invitrogen) according to the manufacturers' protocols. Cells were lysed on ice in Triton lysis buffer (20 mM Tris-HCl [pH 7.4], 135 mM NaCl, 1% Triton X-100, 10% glycerol) supplemented with a protease inhibitor mix (Nacalai Tesque). The samples were boiled in loading buffer and subjected to 5 to 20% gradient sodium dodecyl sulfate-polyacrylamide gel electrophoresis (SDS-PAGE). The proteins were transferred to polyvinylidene difluoride membranes (Millipore, Bedford, MA) and reacted with primary antibody and then secondary horseradish peroxidase-conjugated antibody. The immunocomplexes were visualized with Super Signal West Femto substrate (Pierce, Rockford, IL) and detected by using an LAS-3000 image analyzer (Fujifilm, Tokyo, Japan).

Indirect immunofluorescence assay. Cells cultured on glass slides were fixed with 4% paraformaldehyde in phosphate-buffered saline (PBS) at room temperature for 30 min. After washing three times with PBS, the cells were permeabilized for 20 min at room temperature with PBS containing 0.25% saponin and blocked with phosphate buffer containing 2% bovine serum albumin (BSA) for 1 h at room temperature. The cells were incubated with blocking buffer containing mouse anti-dsRNA, rabbit anti-NS5A, rabbit anti-core, rabbit anti-IRF3, or rabbit anti-STAT2 at room temperature for 1 h, washed three times with PBS, and incubated

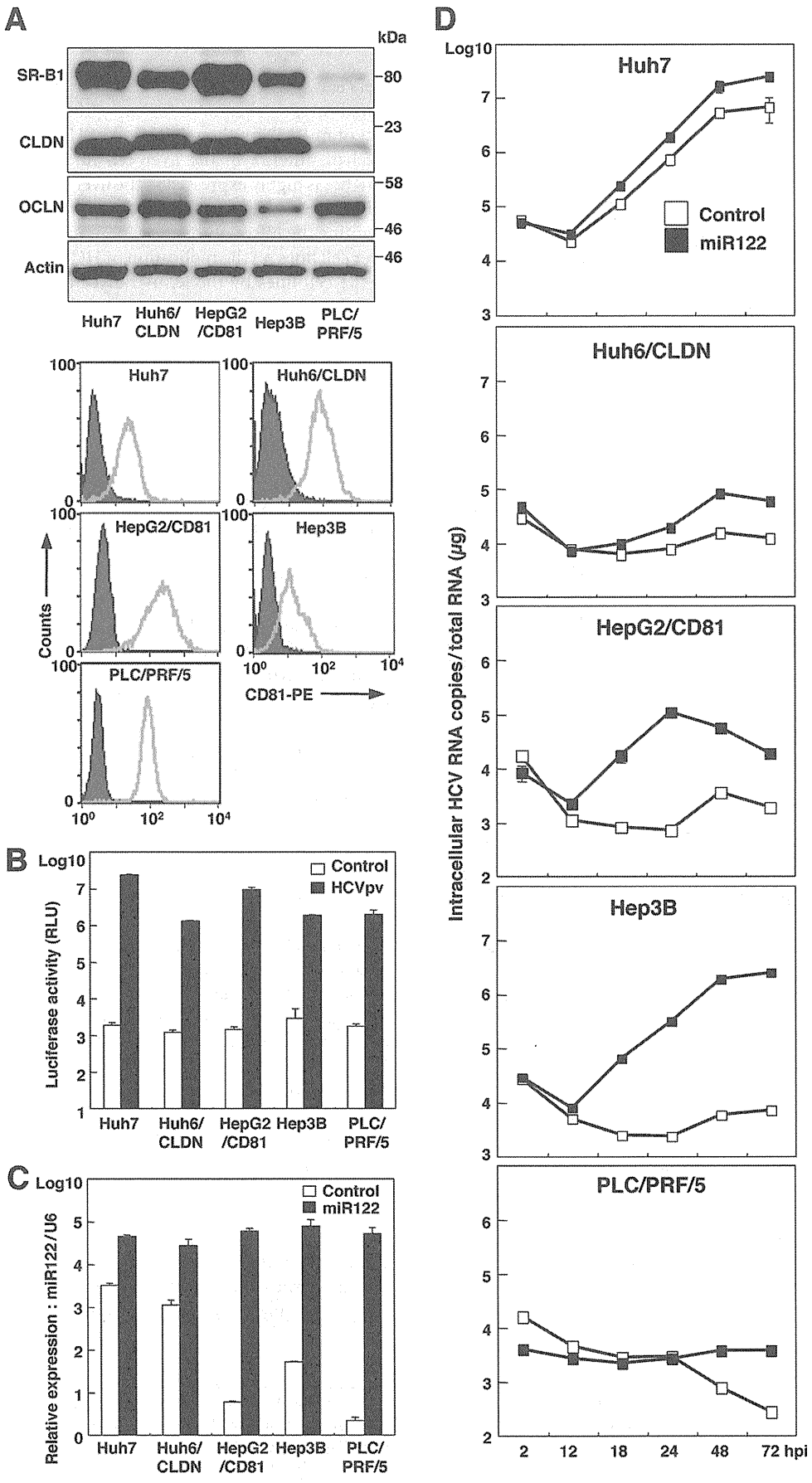
A
kDa
SR-B1
CLDN
OCLN
Actin
80
23
58
46
46
Huh7
Huh6/ CLDN
HepG2 /CD81
Hep3B
PLC/ PRF/5
Huh7
Huh6/CLDN
HepG2/CD81
Hep3B
PLC/PRF/5
Counts
CD81-PE
B
Log10
Control
HCVpv
Luciferase activity (RLU)
C
Log10
Control
miR122
Relative expression : miR122/U6
D
Log10
Huh7
Control
miR122
Huh6/CLDN
HepG2/CD81
Hep3B
PLC/PRF/5
Intracellular HCV RNA copies/total RNA (μg)
2
12
18
24
48
72 hpi

with blocking buffer containing appropriate AF488-conjugated and AF594-conjugated secondary antibodies at room temperature for 1 h. Finally, the cells were washed three times with PBS and observed with a FluoView FV1000 laser scanning confocal microscope (Olympus, Tokyo, Japan).

Flow cytometry. Cultured cells were detached with 0.25% trypsin-EDTA and incubated with PE-conjugated anti-hCD81 antibody or anti-mouse IgG antibody for 1 h at 4°C. After being washed twice with PBS containing 1% BSA, the cells were analyzed by a BD FACSCalibur flow cytometry system (BD Biosciences).

***In vitro* transcription, RNA transfection, and colony formation.** The plasmids pSGR-JFH1 and pFGR-JFH1 were linearized with XbaI and treated with mung bean exonuclease. The linearized DNA was transcribed *in vitro* by using a MEGAscript T7 kit (Applied Biosystems) according to the manufacturer's protocol. The *in vitro*-transcribed RNA (10 μg) was electroporated into Hep3B cells at 10^6 cells/0.4 ml under conditions of 270 V and 960 μF using a Gene Pulser apparatus (Bio-Rad, Hercules, CA) and plated on DMEM containing 10% FCS and NEAA. The medium was replaced with fresh DMEM containing 10% FCS, NEAA, and 400 μg/ml G418 at 24 h posttransfection. The remaining colonies were fixed with 4% paraformaldehyde and stained with crystal violet at 1 month postelectroporation.

Luciferase assay. Cells were seeded onto 24-well plates at a concentration of 5×10^4 cells/well and transfected with 250 ng of each of the plasmids. At 24 h posttransfection, cells were stimulated with the appropriate ligands for 24 h and then lysed in 100 μl of passive lysis buffer (Promega). Luciferase activity was measured in 20-μl aliquots of the cell lysates using a dual-luciferase reporter assay system (Promega). Firefly luciferase activity was standardized with that of *Renilla* luciferase cotransfected with the internal control plasmid pRL-TK and was expressed as RLU.

RESULTS

Expression of miR122 facilitates replication of HCVcc in various liver cell lines. The robust *in vitro* cell culture systems for HCV use the HCV genotype 2a isolate JFH1 and Huh7-derived cell lines (64). To expand the host range of HCVcc to gain more insight into the host-virus interaction, we examined the effect of expression of miR122, a liver-specific microRNA that was shown to be crucial for the efficient replication of HCV (27–29, 38, 52), in several well-characterized liver cell lines: Huh6, HepG2, Hep3B, and PLC/PRF/5. Although hCD81, SR-B1, claudin-1 (CLDN), and occludin (OCLN) are known to be crucial for entry of HCVcc (15, 48, 49, 54), the Huh6 and HepG2 cell lines express little or no CLDN and hCD81 (10, 22), respectively. Therefore, CLDN and hCD81 were exogenously expressed in the cell lines, and the resulting lines were designated Huh6/CLDN and HepG2/CD81, respectively. Expression of the receptor molecules in the cell lines was confirmed by immunoblot and fluorescence-activated cell sorter (FACS) analyses (Fig. 1A). To further examine the susceptibility to HCV infection, pseudotyped VSV bearing the HCV envelope protein, HCVpv, was inoculated into these cell lines. Significant expression of luciferase was observed in these cell lines upon infection with HCVpv but not upon infection with the control virus (Fig. 1B), suggesting that the liver cell lines express functional receptors required for entry of HCV. To determine the effect of miR122 on the replication of HCVcc, we next assessed the level of miR122 in the liver cell lines by qRT-PCR. Although miR122 is highly expressed in the liver (13), the expression level of miR122 varied among the liver cell lines (Fig. 1C, white bars). To examine the effect of the exogenous expression of miR122 in the liver cell lines on the replication of HCVcc, miR122 was expressed in the cell lines by the lentiviral vector. The expression level of miR122 in the liver cell lines, including Huh7 cells, was shown to be upregulated to a significantly greater extent than that in Huh7 cells alone (Fig. 1C, black bars). To examine the effect of miR122 on the replication of HCV, HCVcc was inoculated into the cell lines (Fig. 1D). Although Huh7 cells exhibited an efficient HCV replication, a slight enhancement of the replication was observed by the expression of miR122. No HCV replication was observed in PLC/PRF/5 cells irrespective of miR122 expression. Hep3B and HepG2/CD81 cells exhibited a significant enhancement of HCV replication by the expression of miR122, in contrast to a slight increase in Huh6/CLDN cells. Notably, HCV RNA levels were drastically increased by more than 300-fold at 72 h postinfection in Hep3B cells by the expression of miR122, suggesting that Hep3B is the most suitable cell line for investigating the biological significance of miR122 on the propagation of HCV and for establishing a permissive cell line for HCVcc. Therefore, we used Hep3B cells overexpressing miR122 (Hep3B/miR122 cells) for further experiments.

Expression of biologically active miR122 facilitates replication of HCVcc in Hep3B cells. To confirm the activity of endogenously and exogenously expressed miR122 to suppress the translation in cells, a pmirGLO vector carrying the complementary sequence of miR122 under the luciferase gene was transfected into Huh7 cells, Hep3B cells expressing AcGFP (Hep3B/Cont), and Hep3B/miR122 cells. Suppression of luciferase expression was observed in Huh7 and Hep3B/miR122 cells but not in Hep3B/Cont cells (Fig. 2A), suggesting that miR122 exogenously expressed in Hep3B cells is as biologically active as that endogenously expressed in Huh7 cells. To determine the effect of miR122 on the propagation of HCVcc, Hep3B cells were infected with the lentiviral vector expressing miR122 and then inoculated with HCVcc. The levels of HCV RNA in Hep3B cells upon infection with HCVcc were increased in proportion to the amount of lentiviral vector (Fig. 2B). Recently, an inhibitor for miR122, SPC3649, which is an LNA in which 2′ oxygen and 4′ carbon are connected via methylene units, has been shown to possess potent anti-HCV activity in chimpanzees chronically infected with HCV (31). We next examined the effect of LNA on the replication of HCVcc in Huh7 and Hep3B/miR122 cells. HCV RNA replication in Huh7 and Hep3B/miR122 cells was significantly and dose-dependently decreased by treatment with LNA-miR122 but not treatment with LNA-Cont (Fig. 2C). We further investigated the effect of the

FIG 1 Expression of miR122 facilitates replication of HCVcc in various liver cell lines. (A) Human liver cell lines Huh7, Huh6/CLDN, HepG2/CD81, Hep3B, and PLC/PRF/5 were lysed and subjected to immunoblotting using appropriate antibodies. The expression levels of hCD81 in the liver cell lines were determined by flow cytometry. (B) The human liver cell lines were inoculated with HCVpv or control virus and washed three times after 2 h of incubation. Luciferase activities were determined at 24 h postinfection. (C) The cell lines were transduced with lentiviral vectors expressing miR122 or AcGFP as a control. After serial passages, total RNA was extracted from the cells and relative expression of miR122 was determined by qRT-PCR by using U6 snRNA as an internal control. (D) The cells expressing miR122 or control were infected with HCVcc at an MOI of 1. Total RNA was extracted from the cells at the indicated time and subjected to qRT-PCR analysis. The data are representative of three independent experiments. Error bars indicate the standard deviation of the mean.

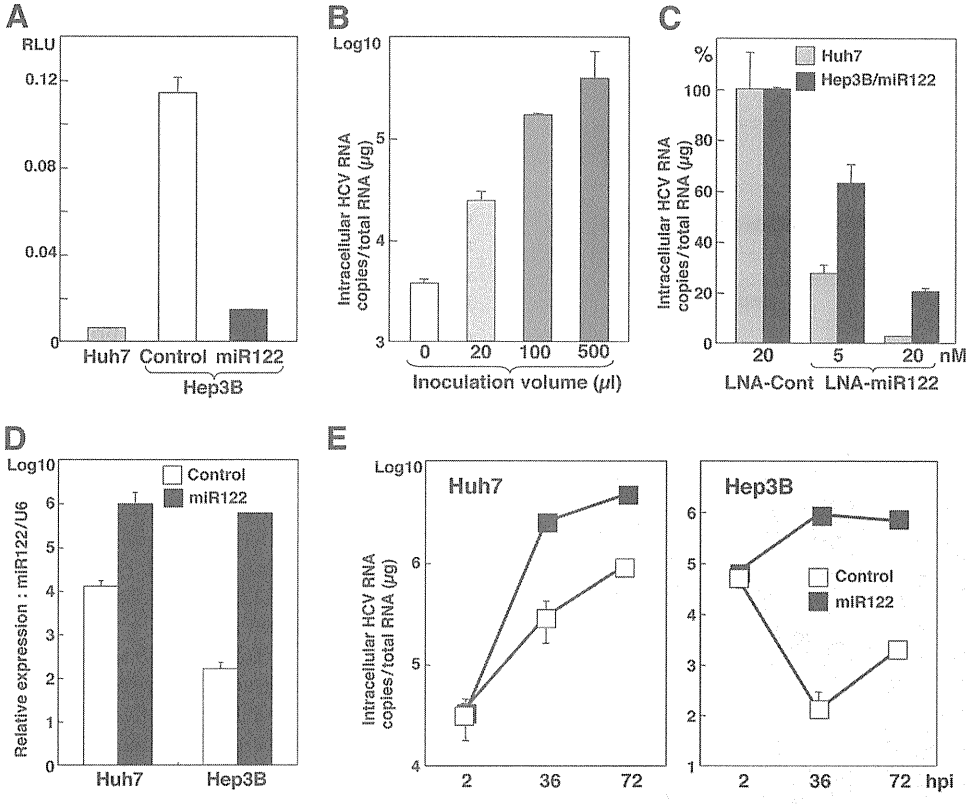

FIG 2 Expression of biologically active miR122 facilitates replication of HCVcc in Hep3B cells. (A) Huh7, Hep3B/Cont, and Hep3B/miR122 cells were transfected with pmirGLO-miR122comp, and luciferase activity was determined at 24 h posttransfection. (B) Hep3B cells were transduced with the lentiviral vector expressing miR122 in a dose-dependent manner and then infected with HCVcc at an MOI of 1 at 48 h postransduction. Total RNA was extracted from the cells at 72 h postinfection and subjected to qRT-PCR. (C) LNA-Cont (20 nM) or LNA-miR122 (5 nM or 20 nM) was introduced into Hep3B/miR122 cells and infected with HCVcc at an MOI of 1 at 12 h posttransfection. Total RNA was extracted from the cells at 24 h postinfection and subjected to qRT-PCR. (D) Huh7 and Hep3B cells were transfected with mimic miR122 (20 nM) or a negative control (20 nM), and total miRNA was determined by qRT-PCR at 24 h posttransfection. (E) Huh7 and Hep3B cells were transfected with mimic miR122 (20 nM) or a negative control (20 nM) and infected with HCVcc at an MOI of 1 at 12 h posttransfection. Total RNA was extracted from the cells at the indicated time (hpi, hours postinfection) and subjected to qRT-PCR.

mimic miR122, the synthetic double-stranded RNA oligonucleotides that mimic endogenous miRNA function, on the propagation of HCV. Huh7 and Hep3B cells transfected with mimic miR122 but not those transfected with the negative control exhibited a high level of expression of miR122 (Fig. 2D) and enhanced RNA replication upon infection with HCVcc (Fig. 2E). Collectively, these results clearly indicate that expression of biologically active miR122 plays a crucial role in the replication of HCV in Hep3B cells.

Establishment of a novel permissive cell line for robust propagation of HCVcc by expression of miR122 in Hep3B cells. We next examined the possibility of establishing a permissive cell line for the robust propagation of HCVcc by the expression of miR122 in Hep3B cells. Huh7, Hep3B/miR122, and Hep3B/Cont cells were infected with HCVcc, and the levels of expression of HCV NS5A and core proteins were assessed by immunoblotting at 72 h postinfection. Expression of the viral proteins in Hep3B/miR122 cells was almost comparable to that in Huh7 cells, in contrast to no expression in Hep3B/Cont cells (Fig. 3A). Small foci stained by immunofluorescence assay appeared at 24 h postinfection in Hep3B/miR122 and Huh7 cells but not in Hep3B/Cont cells and grew into large foci at 72 h postinfection, indicating that infectious particles are generated in Hep3B/miR122 cells and the progeny particles expand infection to the neighboring cells (Fig. 3B). The morphology of Hep3B cells is completely different from that of Huh7 cells, and thus, these results are not due to contamination of Huh7 cells. DGAT1 and ApoE have been shown to play crucial roles in the recruitment of core protein to the lipid droplets and viral infectivity, respectively (9, 24). Higher levels of expression of ApoE and DGAT1 were detected in Hep3B cells than in Huh7 cells (Fig. 3C). Furthermore, the concentration of infectious particles recovered in the culture supernatant of Hep3B/miR122 cells infected with HCVcc at a multiplicity of infection (MOI) of 1 at 72 h postinfection was approximately 5×10^4 FFU/ml, which was comparable to that in Huh7 cells, and was in clear contrast to the significantly lower titer in Hep3B/Cont cells (less than 10 FFU/ml). These results clearly indicate that expression of miR122 in Hep3B cells enables the establishment of a novel permissive cell line for the robust propagation of HCVcc.

Establishment of an HCV RNA replicon in Hep3B/miR122 cells. It has been shown that "cured" cells established through the elimination of the HCV genome from replicon cells by treatment with IFN-α exhibited more potent propagation of HCVcc than the original Huh7 cells (4). To establish a cured cell line derived from Hep3B/miR122 cells for further improvement of HCVcc propagation, we first established HCV replicon cells in Hep3B/miR122 cells. *In vitro*-transcribed sub- or full-genomic HCV RNA of the JFH1 strain was electroporated into Hep3B/miR122 and

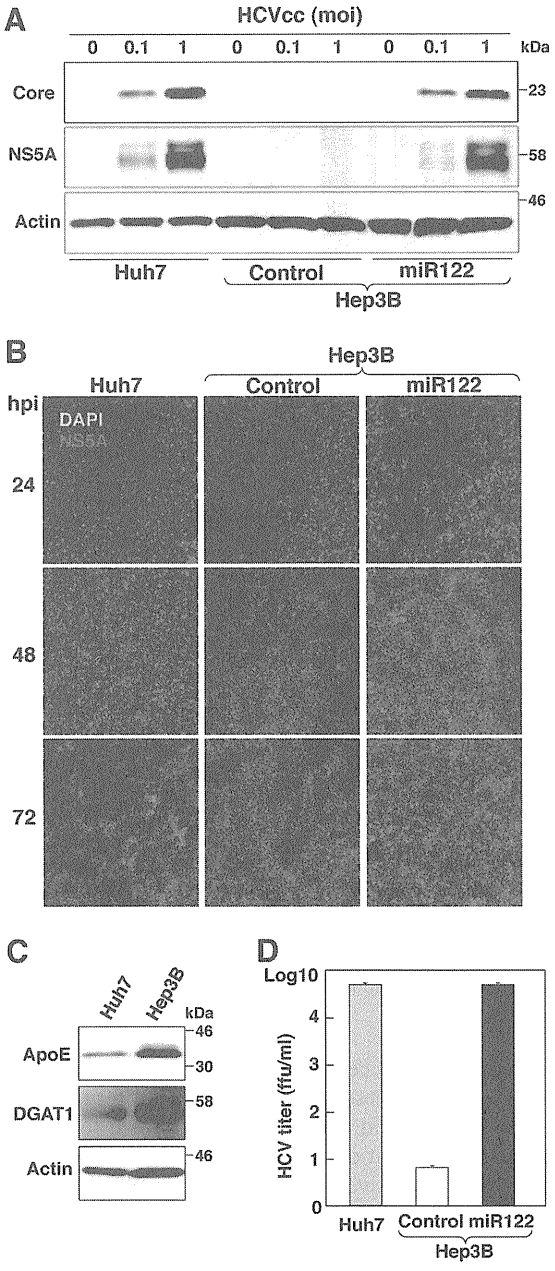

FIG 3 Establishment of a novel permissive cell line for robust propagation of HCVcc by expression of miR122 in Hep3B cells. (A) Huh7, Hep3B/Cont, and Hep3B/miR122 cells were infected with HCVcc at an MOI of 0.1 or 1, and the levels of expression of viral proteins were determined by immunoblotting using appropriate antibodies at 72 h postinfection. (B) Huh7, Hep3B/Cont, and Hep3B/miR122 cells were infected with HCVcc at an MOI of 1 and incubated with 1% methylcellulose in DMEM containing 5% FCS for the indicated time. Cells were fixed with 4% paraformaldehyde and subjected to indirect immunofluorescence assay using anti-NS5A antibody, followed by AF594-conjugated anti-rabbit IgG (red). Cell nuclei were stained with 4′,6-diamidino-2-phenylindole (DAPI; blue). (C) Huh7 and Hep3B cells were lysed and subjected to immunoblotting using appropriate antibodies. (D) Huh7, Hep3B/Cont, and Hep3B/miR122 cells were infected with HCVcc at an MOI of 1, the culture supernatants were collected at 72 h postinfection, and the viral titers of the supernatants were determined by focus-forming assay using Huh7.5.1 cells.

Hep3B/Cont cells, the cells were cultured with 400 μg/ml of G418 for 1 month, and subgenomic replicon (SGR) and full-genomic replicon (FGR) cells were established. Hep3B/miR122 cells electroporated with viral RNA generated a large number of colonies, in contrast to the complete absence of colony formation in Hep3B/Cont cells (Fig. 4A). High levels of HCV RNA comparable to those in the Huh7 cells harboring SGR of the JFH1 strain were detected in Hep3B/miR122 cells harboring either SGR or FGR of the JFH1 strain (Fig. 4B, lower). Expression of NS5A was detected in all of the clones of Hep3B/miR122 cells harboring either SGR or FGR, and that of the core protein was detected in all of the FGR clones (Fig. 4B, upper). HCV core protein and RNA were shown to localize mainly on the lipid droplets and on the cytoplasmic face of ER, respectively (40, 61). Immunofluorescence analyses revealed that dsRNA was colocalized with calnexin, an ER marker, in both SGR and FGR cells and HCV core protein was colocalized with lipid droplets in the FGR cells, as previously described (Fig. 4C). Treatment of Hep3B/miR122 cells harboring an FGR of the JFH1 strain with either CsA or IFN-α decreased the expression of core protein in a dose-dependent manner (Fig. 4D), suggesting that the Hep3B/miR122 replicon cells can be used for screening antiviral compounds for HCV.

Elimination of HCV RNA from HCV replicon RNA from Hep3B/miR122 cells enhances propagation of HCVcc. To establish cured Hep3B/miR122 cells, five clones of the Hep3B/miR122 replicon cells harboring FGR of the JFH1 strain were treated with 100 IU/ml of IFN-α to eliminate viral RNA, and viral RNA was gradually decreased and completely eliminated at 20 days posttreatment (Fig. 5A, left). We then examined the sensitivity of the cured cell clones for propagation of HCVcc. All of the cured cell clones exhibited enhancement of propagation of HCVcc, especially clone 5, which achieved a level of replication of HCVcc more than 6-fold higher than that in the parental Hep3B/miR122 cells (Fig. 5A, right). To examine the effect of serial passage of HCVcc in the cured Hep3B/miR122 cells, HCVcc was inoculated into the cured cells at an MOI of 0.1, and the culture supernatants harvested at 4 days postinfection were reinoculated into the naïve cured cells (Fig. 5B). Infectious titers in the culture supernatants were continuously increased in accord with the number of passages (Fig. 5C). These results indicate that a novel cell line capable of complete propagation of HCVcc was established by the introduction of miR122 and the curing process, as in the case of Huh7 cells by using Hep3B cells.

Cured Hep3B/miR122 cells facilitate efficient propagation of HCVcc through enhanced expression of miR122. It has been reported that one of the reasons for the high susceptibility of the cured cell line Huh7.5 to the propagation of HCVcc is the disruption of the innate immune responses caused by mutation in RIG-I, a key sensor for viral RNA in the cytoplasm (57, 69). To examine the innate immune response in the cured Hep3B/miR122 cells, reporter plasmids encoding the luciferase gene under the control of either the IFN-β (Fig. 6A, left) or ISRE (Fig. 6A, right) promoter were transfected into the cured or parental Hep3B/miR122 cells and stimulated with poly(I·C), VSV, or IFN-α. Activation of these promoters in the cured Hep3B/miR122 cells was not impaired but rather was enhanced upon stimulation with poly(I·C) or VSV compared with that in the parental cells. To further assess the authenticity of viral RNA recognition and ISG induction pathways in the cured Hep3B/miR122 cells, nuclear localization of IRF3 and STAT2 upon stimulation was determined by immuno-

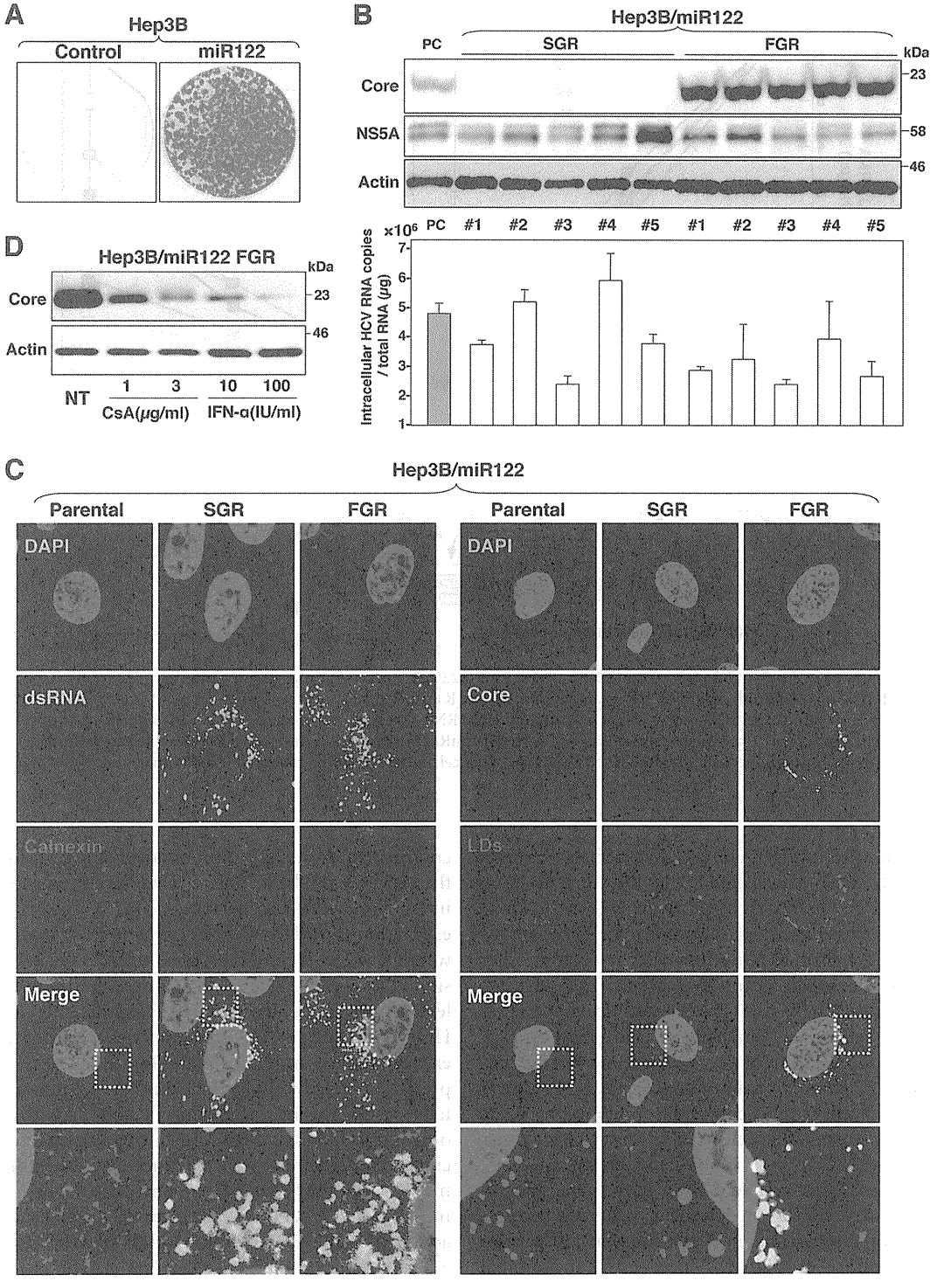

FIG 4 Establishment of an HCV RNA replicon in Hep3B/miR122 cells. (A) Full-genomic replicon RNA of HCV was electroporated into Hep3B/Cont and Hep3B/miR122 cells, and the medium was replaced with DMEM containing 10% FCS and 400 μg/ml G418 at 24 h posttransfection. Colony formation was determined as indicated in Materials and Methods. (B) (Upper) Sub- and full-genomic HCV replicons (SGR and FGR) in Hep3B/miR122 cells were subjected to immunoblotting using the appropriate antibodies. Huh7.5.1 cells infected with HCVcc were used as a positive control (PC). (Lower) Intracellular HCV copy number in replicon clones. SGR in Huh7 cells was used as a positive control. (C) SGR and FGR in Hep3B/miR122 cells were fixed with 4% paraformaldehyde and subjected to indirect immunofluorescence assay using the appropriate antibodies. Lipid droplets (LDs) were stained red with BODIPY. Cell nuclei were stained with 4′,6-diamidino-2-phenylindole (blue). The boxed regions in the merged images are magnified. (D) Hep3B/miR122 FGR cells were treated with DMEM containing 10% FCS and the indicated concentrations of CsA and IFN-α and then subjected to immunoblotting using appropriate antibodies at 48 h posttransfection. NT, no treatment.

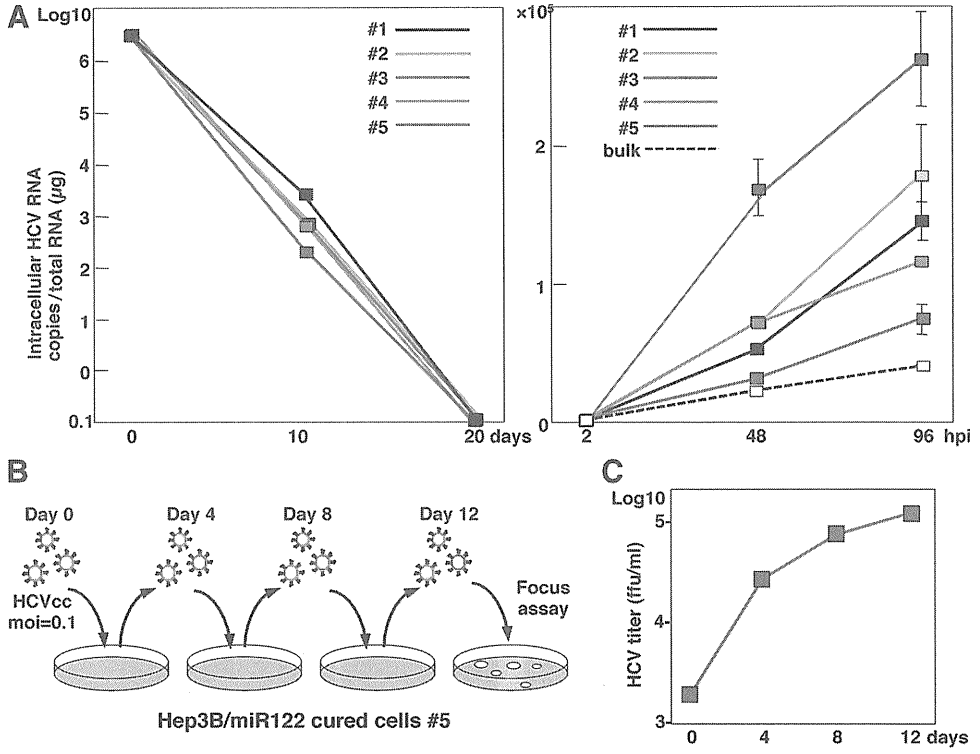

FIG 5 Elimination of HCV RNA from HCV replicon RNA from Hep3B/miR122 cells enhances propagation of HCVcc. (A) (Left) Hep3B/miR122 FGR cell clones were treated with IFN-α (100 IU/ml), and HCV RNA was determined by qRT-PCR at 10 and 20 days posttreatment; (right) Hep3B/miR122 parental cells (bulk) and the cured cells were infected with HCVcc at an MOI of 0.1, and HCV RNA was determined by qRT-PCR at 48 and 96 h postinfection. (B) Schematic diagram of the experimental procedure for serial passage of HCVcc in Hep3B/miR122 cured cells. The cured cells were infected with HCVcc at an MOI of 0.1. (C) The infectious titers in the culture supernatants of the Hep3B/miR122 cured cells were determined at the indicated time points by focus-forming assay using Hep3B/miR122 cells.

fluorescence analysis. IRF3 and STAT2 in both cured and parental Hep3B/miR122 cells were translocated into the nucleus upon stimulation with VSV and IFN-α, respectively (Fig. 6B). These results suggest that the efficient propagation of HCVcc in the cured Hep3B/miR122 cells might be attributable to reasons other than impairment of the innate immune response. Therefore, we hypothesized that the Hep3B/miR122 cells harboring the HCV genome are capable of surviving in the presence of a high concentration of G418 by amplification of the viral genome through enhancement of miR122 expression and that once HCV RNA was eliminated, the cured cells would acquire the ability to propagate HCV due to the high expression of miR122. To test this hypothesis, the levels of miR122 in both Huh7- and Hep3B/miR122-derived cured cells were compared with those in the parental cells. Intriguingly, both cured cell lines exhibited a significant increase of miR122 expression (approximately 2- to 6-fold) in comparison with that in the parental cells (Fig. 6C). These results suggest that the efficient propagation of HCVcc in the cured Hep3B/miR122 cells was partially attributable to an enhanced expression of miR122, rather than an impairment of the signaling pathway of innate immunity.

Specific interaction of miR122 with viral RNA is crucial for efficient propagation of HCVcc. To evaluate the effect of a specific interaction of miR122 with the target sequence in the 5′ UTR of HCV RNA on the enhancement of viral propagation, we generated two mutant pre-miR122s: sMT-miR122 has a substitution of uridine to adenosine, and dMT-miR122 carries an additional complementary substitution of adenosine to uridine to stabilize the expression. These substitutions have been shown to abrogate interaction with the target sequence (27) (Fig. 7A). A high level of expression of dMT-miR122 comparable to that of WT-miR122 was detected in Hep3B cells, in contrast to the low level of expression of sMT-miR122 (Fig. 7B). As described above, the expression level of miR122 in Hep3B cells was significantly lower than that in Huh7 cells (Fig. 1B). Taking advantage of this low level of miR122 expression, WT-miR122 and dMT-miR122 were exogenously expressed in Hep3B cells by the lentiviral vector to assess the importance of the specific interaction of miR122 with viral RNA. Not only intracellular viral RNA levels but also infectious titers in the culture supernatants were enhanced by the expression of WT-miR122, but they were not enhanced by the expression of dMT-miR122 (Fig. 7C and D). These results suggest that specific interaction of miR122 with the 5′ UTR of HCV is crucial for the efficient replication and propagation of HCV.

DISCUSSION

Most miRNAs utilize the normal RNA interfering pathway and repress translation of the target mRNAs (3, 26). For instance, miR122 targets the 3′ UTR of the cytoplasmic polyadenylation element binding protein (CPEB) (5), hemochromatosis (*Hfe*) and hemojuvelin (*Hjv*) (6), a disintegrin and metalloprotease family 10 (ADAM10) (2), and cationic amino transporter 1 (CAT-1) (8) and represses their translation. In contrast, HCV uniquely exploits the liver-specific miR122 to stimulate viral translation (23, 27–29,

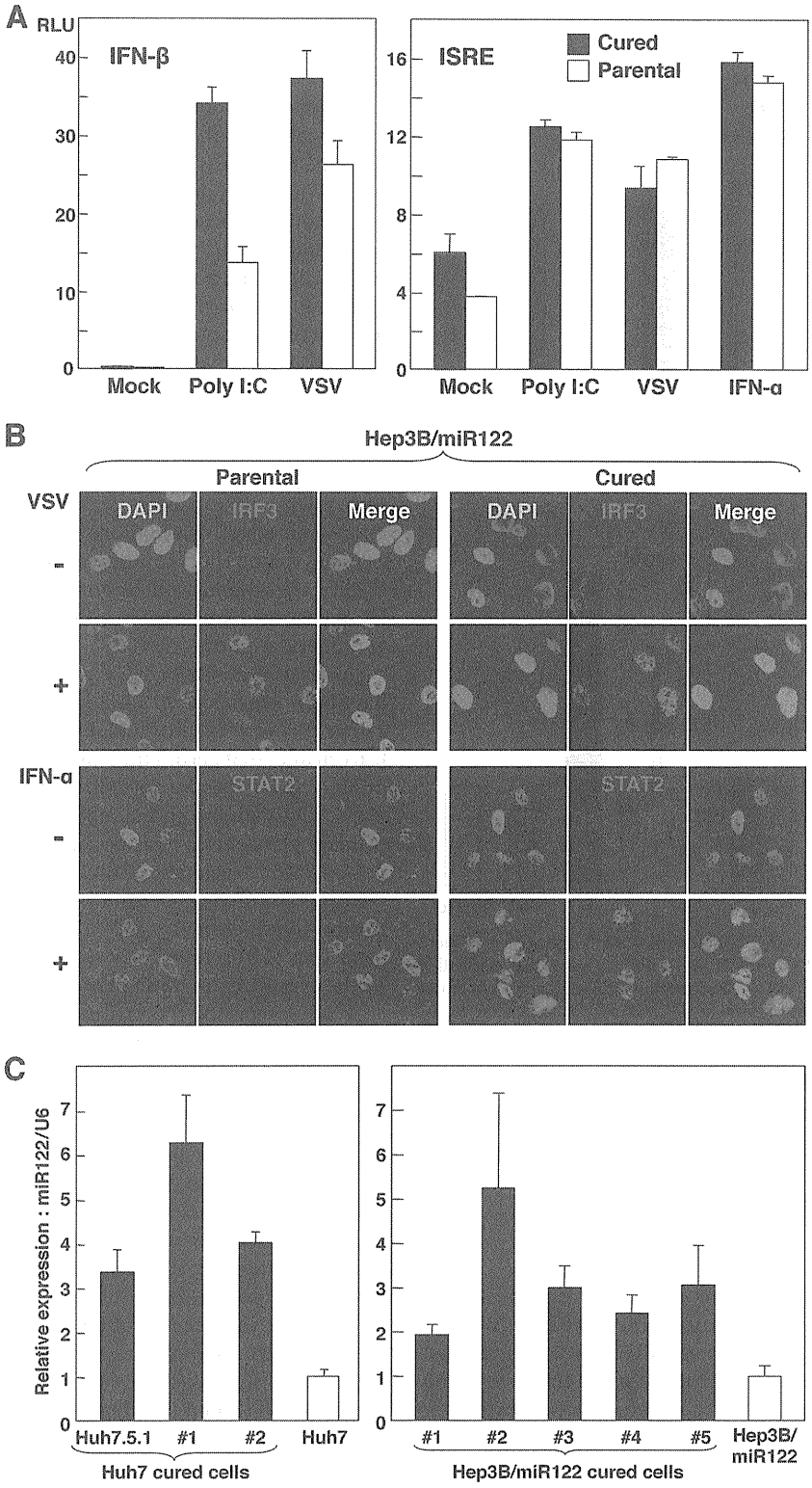

FIG 6 Cured Hep3B/miR122 cells facilitate efficient propagation of HCVcc through enhanced expression of miR122. (A) (Left) Hep3B/miR122 parental cells and cured cells of clone 5 were cotransfected with pIFNβ-Luc and pRL-TK and then infected with the VSV NCP mutant at an MOI of 0.01 or transfected with 1 μg of poly(I·C) at 24 h posttransfection, and luciferase activities were determined at 48 h posttreatment; (right) the cells were cotransfected with pISRE-Luc and pRL-TK and then infected with VSV at an MOI of 0.01 or treated with IFN-α (100 IU/ml) at 24 h posttransfection, and luciferase activities were determined at 48 h posttreatment. (B) (Upper) Hep3B/miR122 parental cells and the cured cells were infected with VSV at an MOI of 0.01, fixed with 4% phosphonoformic acid at 18 h postinfection, and subjected to indirect immunofluorescence assay using rabbit anti-IRF3 antibody, followed by AF488-conjugated anti-rabbit IgG (red); (lower) the cells were treated with IFN-α (100 IU/ml), fixed with 4% paraformaldehyde at 1 h postinfection, and subjected to indirect immunofluorescence assay using rabbit anti-STAT2 antibody, followed by AF488-conjugated anti-rabbit IgG (red). Cell nuclei were stained with 4′,6-diamidino-2-phenylindole (blue). (C) Total RNA was extracted from parental Huh7 and Hep3B/miR122 cells and their cured cells, and the relative expression of miR122 was determined by qRT-PCR by using U6 snRNA as an internal control.

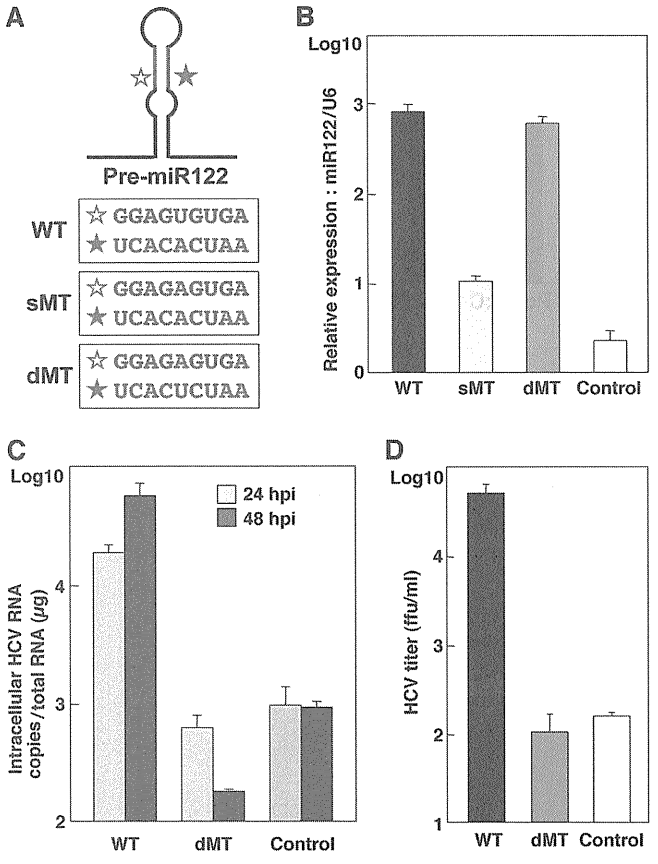

FIG 7 Specific interaction of miR122 with viral RNA is crucial for efficient propagation of HCVcc. (A) Diagram of pre-miR122 and partial nucleotide sequences of wild type (WT) miR122 and mutant miR122 carrying a single mutation (sMT) and double mutations (dMT). (B) Hep3B cells were transduced with lentiviral vectors expressing either WT-, sMT-, or dMT-miR122 or with a control, and the relative expression of miR122 was determined by qRT-PCR by using U6 snRNA as an internal control. (C) Hep3B cells expressing WT- or dMT-miR122 or the control cells were infected with HCVcc at an MOI of 1, and the level of HCV RNA was determined by qRT-PCR at 24 and 48 h postinfection. (D) The culture supernatants were collected at 72 h postinfection, and the viral titers of the supernatants were determined by focus-forming assay using Huh7.5.1 cells.

38, 52). In this study, we assessed the possibility of establishment of human liver cell lines that are susceptible to HCVcc propagation through exogenous expression of miR122 by a lentiviral vector. Although Huh7 cells and their derived cell lines are highly susceptible to propagation of HCVcc, they intrinsically express an abundant amount of miR122. Among the cell lines that we investigated, Hep3B cells exhibit a high sensitivity to HCVcc propagation by expression of miR122 compared to that of Huh7 cells, whereas no sensitivity to HCVcc was observed in the parental Hep3B cells. Therefore, the Hep3B cell line was suggested to be an ideal tool to investigate miR122 function in the life cycle of HCV.

RNA viruses replicate in host cells with high error rates, generating a broad population diversity, which allows rapid adaptation to new environments (33). HCV propagates in the liver of patients with quasispecies heterogeneity and transmits to a new host through contaminated blood or blood products (16). It is known that the complexity of HCV clones significantly decreases during transmission through a genetic bottleneck, resulting in a more homogeneous population. This selection of certain clones is mainly caused by the host factors required for viral replication and immune pressure in a new host and is involved in the early phase of HCV infection in the new environment (18, 25, 32). A sole cell line, Huh7, has been employed in most of the experiments for *in vitro* studies of entry, RNA replication, and particle formation of HCV. Therefore, it has not been possible to assess propagation of HCVcc in human liver cell lines other than Huh7 cells and transmission of HCVcc to liver cell lines of different origins. The establishment of a novel human liver cell line, Hep3B/miR122, for propagation of HCVcc would help to generate new insights into the mutual interaction between HCV and human hepatocytes. Although we are not able to evaluate the effects of the acquired immunity on the induction of the adaptive mutations in cell culture systems, we can assess the host factors involved in the generation of the adaptive mutations by using two different human liver cell lines that support continuous propagation of HCVcc. Further studies are needed to determine the adaptive mutations in the HCV genome by passage in either Hep3B/miR122 or Huh7 cells and in one after the other.

At least seven major HCV genotypes and numerous subtypes have been identified (21), but laboratory strains capable of replicating *in vitro* are limited (36, 64, 68, 70). It is important to establish cell lines that permit the complete propagation of a wide range of HCV genotypes for further understanding of the life cycle of HCV. Although the partial replication of serum-derived HCV in primary hepatocytes in a specialized culture system has been reported (50), development of a simpler and more user-friendly system is required for promotion of research on HCV. It might be feasible to establish new cell culture systems for not only various genotypes of infectious HCV clones but also serum-derived HCV by the expression of miR122 in various human liver cell lines.

While preparing the manuscript, Narbus et al. reported that the expression of miR122 enhances HCV replication in HepG2/CD81 cells (46). Our data also demonstrated that the expression of miR122 increased HCV replication in HepG2/CD81 cells, as shown in Fig. 1D. However, the impact of miR122 expression on the production of infectious particles in HepG2/CD81 cells is significantly lower than that in Huh7 cells (46). Although LH86 (71) and Li23 (30) cell lines derived from human hepatocellular carcinoma have been shown to permit propagation of HCVcc, these cell lines are not well characterized. In contrast, the Hep3B cell line has been utilized in a wide range of research fields for a long time, resulting in the accumulation of many sources of data from genomic and proteomic analyses (1, 47, 55, 63, 67). Moreover, the Hep3B cell line is available from the major cell banks all over the world, which should readily allow reevaluation of the findings in this study. Comparison of the experimental data on HCVcc propagation between Huh7 and Hep3B/miR122 cells might provide a clue to understanding the host factors crucial for the efficient propagation of HCV in human liver cells.

The higher susceptibility to HCVcc propagation of the cured cells derived from Huh7 cells than the parental cells was suggested to be attributable to impairment of the innate immune response (57). However, this is not the only reason for efficient propagation of HCVcc in the Huh7-based cured cell lines (17). It has been shown that cured cell lines, such as Huh7.5.1 and Huh7-Lunet, express a higher level of miR122 than the parental Huh7 cells (13), suggesting that upregulation of miR122 in the cured cells participates in the efficient propagation of HCVcc. However, the level of

miR122 expression in the cured Hep3B cells was not necessarily correlated with the replication efficiency of HCVcc in the present work (Fig. 6C). Most recently, Denard et al. reported that the expression of CREB3L1/OASIS, which specifically prevents division of virus-infected cells, in cured Huh7 cells was reduced compared to that in the parental cells (12), suggesting that CREB3L1/OASIS is also involved in the enhancement of HCVcc propagation in the cured cells.

In this study, we have shown that expression of miR122 confers susceptibility to human liver cell lines for the efficient propagation of HCVcc. Elimination of the HCV genome from the replicon cells of Hep3B/miR122 cells enhanced propagation of HCVcc in accord with the increment of miR122 expression, and propagation of HCVcc in the cured cells was continuously increased in every passage. Furthermore, the interaction between HCV RNA and miR122 was shown to be specific for production of infectious particles in Hep3B/miR122 cells. The establishment of a new permissive cell line for HCVcc allows us not only to investigate the biological function of miR122 on the life cycle of HCV but also to develop novel therapeutics for chronic hepatitis C.

ACKNOWLEDGMENTS

We thank M. Tomiyama for her secretarial work. We also thank M. Hijikata, T. Wakita, F. Chisari, T. Kawai, S. Akira, and M. Whitt for providing experimental materials.

This work was supported in part by grants-in-aid from the Ministry of Health, Labor, and Welfare (Research on Hepatitis); the Ministry of Education, Culture, Sports, Science, and Technology; and the Osaka University Global Center of Excellence Program.

REFERENCES

1. **Aden DP, Fogel A, Plotkin S, Damjanov I, Knowles BB.** 1979. Controlled synthesis of HBsAg in a differentiated human liver carcinoma-derived cell line. Nature **282**:615–616.
2. **Bai S, et al.** 2009. MicroRNA-122 inhibits tumorigenic properties of hepatocellular carcinoma cells and sensitizes these cells to sorafenib. J. Biol. Chem. **284**:32015–32027.
3. **Bartel DP.** 2009. MicroRNAs: target recognition and regulatory functions. Cell **136**:215–233.
4. **Blight KJ, McKeating JA, Rice CM.** 2002. Highly permissive cell lines for subgenomic and genomic hepatitis C virus RNA replication. J. Virol. **76**: 13001–13014.
5. **Burns DM, D'Ambrogio A, Nottrott S, Richter JD.** 2011. CPEB and two poly(A) polymerases control miR-122 stability and p53 mRNA translation. Nature **473**:105–108.
6. **Castoldi M, et al.** 2011. The liver-specific microRNA miR-122 controls systemic iron homeostasis in mice. J. Clin. Invest. **121**:1386–1396.
7. **Chang J, et al.** 2008. Liver-specific microRNA miR-122 enhances the replication of hepatitis C virus in nonhepatic cells. J. Virol. **82**:8215–8223.
8. **Chang J, et al.** 2004. miR-122, a mammalian liver-specific microRNA, is processed from hcr mRNA and may downregulate the high affinity cationic amino acid transporter CAT-1. RNA Biol. **1**:106–113.
9. **Chang KS, Jiang J, Cai Z, Luo G.** 2007. Human apolipoprotein E is required for infectivity and production of hepatitis C virus in cell culture. J. Virol. **81**:13783–13793.
10. **Cormier EG, et al.** 2004. CD81 is an entry coreceptor for hepatitis C virus. Proc. Natl. Acad. Sci. U. S. A. **101**:7270–7274.
11. **Date T, et al.** 2004. Genotype 2a hepatitis C virus subgenomic replicon can replicate in HepG2 and IMY-N9 cells. J. Biol. Chem. **279**: 22371–22376.
12. **Denard B, et al.** 2011. The membrane-bound transcription factor CREB3L1 is activated in response to virus infection to inhibit proliferation of virus-infected cells. Cell Host Microbe **10**:65–74.
13. **Ehrhardt M, et al. 18 April** 2011. Profound differences of microRNA expression patterns in hepatocytes and hepatoma cell lines commonly used in hepatitis C virus studies. Hepatology. [Epub ahead of print.]
14. **Elmen J, et al.** 2008. LNA-mediated microRNA silencing in non-human primates. Nature **452**:896–899.
15. **Evans MJ, et al.** 2007. Claudin-1 is a hepatitis C virus co-receptor required for a late step in entry. Nature **446**:801–805.
16. **Farci P, et al.** 2000. The outcome of acute hepatitis C predicted by the evolution of the viral quasispecies. Science **288**:339–344.
17. **Feigelstock DA, Mihalik KB, Kaplan G, Feinstone SM.** 2010. Increased susceptibility of Huh7 cells to HCV replication does not require mutations in RIG-I. Virol. J. **7**:44.
18. **Feliu A, Gay E, Garcia-Retortillo M, Saiz JC, Forns X.** 2004. Evolution of hepatitis C virus quasispecies immediately following liver transplantation. Liver Transpl. **10**:1131–1139.
19. **Ge D, et al.** 2009. Genetic variation in IL28B predicts hepatitis C treatment-induced viral clearance. Nature **461**:399–401.
20. **Gentzsch J, et al.** 2011. Hepatitis C virus complete life cycle screen for identification of small molecules with pro- or antiviral activity. Antiviral Res. **89**:136–148.
21. **Gottwein JM, et al.** 2009. Development and characterization of hepatitis C virus genotype 1-7 cell culture systems: role of CD81 and scavenger receptor class B type I and effect of antiviral drugs. Hepatology **49**: 364–377.
22. **Haid S, Windisch MP, Bartenschlager R, Pietschmann T.** 2010. Mouse-specific residues of claudin-1 limit hepatitis C virus genotype 2a infection in a human hepatocyte cell line. J. Virol. **84**:964–975.
23. **Henke JI, et al.** 2008. microRNA-122 stimulates translation of hepatitis C virus RNA. EMBO J. **27**:3300–3310.
24. **Herker E, et al.** 2010. Efficient hepatitis C virus particle formation requires diacylglycerol acyltransferase-1. Nat. Med. **16**:1295–1298.
25. **Hughes MG, Jr, et al.** 2005. HCV infection of the transplanted liver: changing CD81 and HVR1 variants immediately after liver transplantation. Am. J. Transplant. **5**:2504–2513.
26. **Huntzinger E, Izaurralde E.** 2011. Gene silencing by microRNAs: contributions of translational repression and mRNA decay. Nat. Rev. Genet. **12**:99–110.
27. **Jangra RK, Yi M, Lemon SM.** 2010. Regulation of hepatitis C virus translation and infectious virus production by the microRNA miR-122. J. Virol. **84**:6615–6625.
28. **Jopling CL, Schutz S, Sarnow P.** 2008. Position-dependent function for a tandem microRNA miR-122-binding site located in the hepatitis C virus RNA genome. Cell Host Microbe **4**:77–85.
29. **Jopling CL, Yi M, Lancaster AM, Lemon SM, Sarnow P.** 2005. Modulation of hepatitis C virus RNA abundance by a liver-specific microRNA. Science **309**:1577–1581.
30. **Kato N, et al.** 2009. Efficient replication systems for hepatitis C virus using a new human hepatoma cell line. Virus Res. **146**:41–50.
31. **Lanford RE, et al.** 2010. Therapeutic silencing of microRNA-122 in primates with chronic hepatitis C virus infection. Science **327**:198–201.
32. **Laskus T, et al.** 2004. Analysis of hepatitis C virus quasispecies transmission and evolution in patients infected through blood transfusion. Gastroenterology **127**:764–776.
33. **Lauring AS, Andino R.** 2010. Quasispecies theory and the behavior of RNA viruses. PLoS Pathog. **6**:e1001005.
34. **Lavanchy D.** 2009. The global burden of hepatitis C. Liver Int. **29**(Suppl. 1):74–81.
35. **Lin LT, et al.** 2010. Replication of subgenomic hepatitis C virus replicons in mouse fibroblasts is facilitated by deletion of interferon regulatory factor 3 and expression of liver-specific microRNA 122. J. Virol. **84**: 9170–9180.
36. **Lindenbach BD, et al.** 2005. Complete replication of hepatitis C virus in cell culture. Science **309**:623–626.
37. **Lohmann V, et al.** 1999. Replication of subgenomic hepatitis C virus RNAs in a hepatoma cell line. Science **285**:110–113.
38. **Machlin ES, Sarnow P, Sagan SM.** 2011. Masking the 5′ terminal nucleotides of the hepatitis C virus genome by an unconventional microRNA-target RNA complex. Proc. Natl. Acad. Sci. U. S. A. **108**:3193–3198.
39. **Masaki T, et al.** 2010. Production of infectious hepatitis C virus by using RNA polymerase I-mediated transcription. J. Virol. **84**:5824–5835.
40. **Miyanari Y, et al.** 2007. The lipid droplet is an important organelle for hepatitis C virus production. Nat. Cell Biol. **9**:1089–1097.
41. **Moradpour D, Penin F, Rice CM.** 2007. Replication of hepatitis C virus. Nat. Rev. Microbiol. **5**:453–463.
42. **Moriishi K, Matsuura Y.** 2007. Evaluation systems for anti-HCV drugs. Adv. Drug Deliv. Rev. **59**:1213–1221.

43. **Moriishi K, Matsuura Y.** 2007. Host factors involved in the replication of hepatitis C virus. Rev. Med. Virol. **17**:343–354.
44. **Moriishi K, Matsuura Y.** 2003. Mechanisms of hepatitis C virus infection. Antivir. Chem. Chemother. **14**:285–297.
45. **Moriishi K, et al.** 2010. Involvement of PA28gamma in the propagation of hepatitis C virus. Hepatology **52**:411–420.
46. **Narbus CM, et al.** 2011. HepG2 cells expressing microRNA miR-122 support the entire hepatitis C virus life cycle. J. Virol. **85**:12087–12092.
47. **Park JG, et al.** 1995. Characterization of cell lines established from human hepatocellular carcinoma. Int. J. Cancer **62**:276–282.
48. **Pileri P, et al.** 1998. Binding of hepatitis C virus to CD81. Science **282**: 938–941.
49. **Ploss A, et al.** 2009. Human occludin is a hepatitis C virus entry factor required for infection of mouse cells. Nature **457**:882–886.
50. **Ploss A, et al.** 2010. Persistent hepatitis C virus infection in microscale primary human hepatocyte cultures. Proc. Natl. Acad. Sci. U. S. A. **107**: 3141–3145.
51. **Randall G, et al.** 2007. Cellular cofactors affecting hepatitis C virus infection and replication. Proc. Natl. Acad. Sci. U. S. A. **104**:12884–12889.
52. **Roberts AP, Lewis AP, Jopling CL.** 2011. miR-122 activates hepatitis C virus translation by a specialized mechanism requiring particular RNA components. Nucleic Acids Res. **39**:7716–7729.
53. **Russell RS, et al.** 2008. Advantages of a single-cycle production assay to study cell culture-adaptive mutations of hepatitis C virus. Proc. Natl. Acad. Sci. U. S. A. **105**:4370–4375.
54. **Scarselli E, et al.** 2002. The human scavenger receptor class B type I is a novel candidate receptor for the hepatitis C virus. EMBO J. **21**:5017–5025.
55. **Seow TK, Liang RC, Leow CK, Chung MC.** 2001. Hepatocellular carcinoma: from bedside to proteomics. Proteomics **1**:1249–1263.
56. **Skalsky RL, Cullen BR.** 2010. Viruses, microRNAs, and host interactions. Annu. Rev. Microbiol. **64**:123–141.
57. **Sumpter R, Jr, et al.** 2005. Regulating intracellular antiviral defense and permissiveness to hepatitis C virus RNA replication through a cellular RNA helicase, RIG-I. J. Virol. **79**:2689–2699.
58. **Suppiah V, et al.** 2009. IL28B is associated with response to chronic hepatitis C interferon-alpha and ribavirin therapy. Nat. Genet. **41**: 1100–1104.
59. **Tanaka Y, et al.** 2009. Genome-wide association of IL28B with response to pegylated interferon-alpha and ribavirin therapy for chronic hepatitis C. Nat. Genet. **41**:1105–1109.
60. **Tani H, et al.** 2007. Replication-competent recombinant vesicular stomatitis virus encoding hepatitis C virus envelope proteins. J. Virol. **81**: 8601–8612.
61. **Targett-Adams P, Boulant S, McLauchlan J.** 2008. Visualization of double-stranded RNA in cells supporting hepatitis C virus RNA replication. J. Virol. **82**:2182–2195.
62. **Thomas DL, et al.** 2009. Genetic variation in IL28B and spontaneous clearance of hepatitis C virus. Nature **461**:798–801.
63. **Vannucchi AM, et al.** 1993. Effects of cyclosporin A on erythropoietin production by the human Hep3B hepatoma cell line. Blood **82**:978–984.
64. **Wakita T, et al.** 2005. Production of infectious hepatitis C virus in tissue culture from a cloned viral genome. Nat. Med. **11**:791–796.
65. **Walters KA, et al.** 2006. Host-specific response to HCV infection in the chimeric SCID-beige/Alb-uPA mouse model: role of the innate antiviral immune response. PLoS Pathog. **2**:e59.
66. **Windisch MP, et al.** 2005. Dissecting the interferon-induced inhibition of hepatitis C virus replication by using a novel host cell line. J. Virol. **79**: 13778–13793.
67. **Wong N, et al.** 2005. Transcriptional profiling identifies gene expression changes associated with IFN-alpha tolerance in hepatitis C-related hepatocellular carcinoma cells. Clin. Cancer Res. **11**:1319–1326.
68. **Yi M, Villanueva RA, Thomas DL, Wakita T, Lemon SM.** 2006. Production of infectious genotype 1a hepatitis C virus (Hutchinson strain) in cultured human hepatoma cells. Proc. Natl. Acad. Sci. U. S. A. **103**: 2310–2315.
69. **Yoneyama M, et al.** 2004. The RNA helicase RIG-I has an essential function in double-stranded RNA-induced innate antiviral responses. Nat. Immunol. **5**:730–737.
70. **Zhong J, et al.** 2005. Robust hepatitis C virus infection in vitro. Proc. Natl. Acad. Sci. U. S. A. **102**:9294–9299.
71. **Zhu H, et al.** 2007. Hepatitis C virus triggers apoptosis of a newly developed hepatoma cell line through antiviral defense system. Gastroenterology **133**:1649–1659.

JOURNAL OF VIROLOGY, Dec. 2011, p. 13185–13194 Vol. 85, No. 24
0022-538X/11/$12.00 doi:10.1128/JVI.06099-11

Dysfunction of Autophagy Participates in Vacuole Formation and Cell Death in Cells Replicating Hepatitis C Virus▽§

Shuhei Taguwa,[1]† Hiroto Kambara,[1]† Naonobu Fujita,[2] Takeshi Noda,[2] Tamotsu Yoshimori,[2] Kazuhiko Koike,[3] Kohji Moriishi,[4] and Yoshiharu Matsuura[1]*

Department of Molecular Virology, Research Institute for Microbial Diseases,[1] and Department of Genetics, Graduate School of Medicine,[2] Osaka University, Osaka 565-0871, Department of Gastroenterology, Graduate School of Medicine, University of Tokyo, Tokyo 113-8655,[3] and Department of Microbiology, Faculty of Medicine, Yamanashi University, Yamanashi 409-3898,[4] Japan

Received 22 August 2011/Accepted 4 October 2011

Hepatitis C virus (HCV) is a major cause of chronic liver diseases. A high risk of chronicity is the major concern of HCV infection, since chronic HCV infection often leads to liver cirrhosis and hepatocellular carcinoma. Infection with the HCV genotype 1 in particular is considered a clinical risk factor for the development of hepatocellular carcinoma, although the molecular mechanisms of the pathogenesis are largely unknown. Autophagy is involved in the degradation of cellular organelles and the elimination of invasive microorganisms. In addition, disruption of autophagy often leads to several protein deposition diseases. Although recent reports suggest that HCV exploits the autophagy pathway for viral propagation, the biological significance of the autophagy to the life cycle of HCV is still uncertain. Here, we show that replication of HCV RNA induces autophagy to inhibit cell death. Cells harboring an HCV replicon RNA of genotype 1b strain Con1 but not of genotype 2a strain JFH1 exhibited an incomplete acidification of the autolysosome due to a lysosomal defect, leading to the enhanced secretion of immature cathepsin B. The suppression of autophagy in the Con1 HCV replicon cells induced severe cytoplasmic vacuolation and cell death. These results suggest that HCV harnesses autophagy to circumvent the harmful vacuole formation and to maintain a persistent infection. These findings reveal a unique survival strategy of HCV and provide new insights into the genotype-specific pathogenicity of HCV.

Hepatitis C virus (HCV) is a major causative agent of bloodborne hepatitis and currently infects at least 180 million people worldwide (58). The majority of individuals infected with HCV develop chronic hepatitis, which eventually leads to liver cirrhosis and hepatocellular carcinoma (25, 48). In addition, HCV infection is known to induce extrahepatic diseases such as type 2 diabetes and malignant lymphoma (20). It is believed that the frequency of development of these diseases varies among viral genotypes (14, 51). However, the precise mechanism of the genotype-dependent outcome of HCV-related diseases has not yet been elucidated. Despite HCV's status as a major public health problem, the current therapy with pegylated interferon and ribavirin is effective in only around 50% of patients with genotype 1, which is the most common genotype worldwide, and no effective vaccines for HCV are available (35, 52). Although recently approved protease inhibitors for HCV exhibited a potent antiviral efficacy in patients with genotype 1 (36, 43), the emergence of drug-resistant mutants is a growing problem (16). Therefore, it is important to clarify the life cycle and pathogenesis of HCV for the development of more potent remedies for chronic hepatitis C.

* Corresponding author. Mailing address: Department of Molecular Virology, Research Institute for Microbial Diseases, Osaka University, 3-1, Yamadaoka, Suita-shi, Osaka 565-0871, Japan. Phone: 81-6-6879-8340. Fax: 81-6-6879-8269. E-mail: matsuura@biken.osaka-u.ac.jp.
† These authors contributed equally to this work.
§ Supplemental material for this article may be found at http://jvi.asm.org/.
▽ Published ahead of print on 12 October 2011.

HCV belongs to the genus *Hepacivirus* of the family *Flaviviridae* and possesses a single positive-stranded RNA genome with a nucleotide length of 9.6 kb, which encodes a single polyprotein consisting of approximately 3,000 amino acids (40). The precursor polyprotein is processed by host and viral proteases into structural and nonstructural (NS) proteins (34). Not only viral proteins but also several host factors are required for efficient replication of the HCV genome, where NS5A is known to recruit various host proteins and to form replication complexes with other NS proteins (39). In the HCV-propagating cell, host intracellular membranes are reconstructed for the viral niche known as the membranous web, where it is thought that progeny viral RNA and proteins are concentrated for efficient replication and are protected from defensive degradation, as are the host protease and nucleases (38).

Autophagy is a bulk degradation process, wherein portions of cytoplasm and organelles are enclosed by a unique membrane structure called an autophagosome, which subsequently fuses with the lysosome for degradation (37, 60). Autophagy occurs not only in order to recycle amino acids during starvation but also to clear away deteriorated proteins or organelles irrespective of nutritional stress. In fact, the deficiency of autophagy leads to the accumulation of disordered proteins that can ultimately cause a diverse range of diseases, including neurodegeneration and liver injury (12, 29, 30), and often to type 2 diabetes and malignant lymphoma (9, 32).

Recently, it has been shown that autophagy is provoked upon replication of several RNA viruses and is closely related to their propagation and/or pathogenesis. Coxsackievirus B3

utilizes autophagic membrane as a site of genome replication, whereas influenza virus attenuates apoptosis through the induction of autophagy (10, 59). Moreover, several groups have reported that HCV induces autophagy for infection or replication (5, 49); however, the role(s) of autophagy in the propagation of HCV is still controversial and the involvement of autophagy in the pathogenesis of HCV has not yet been clarified. In this study, we examined the biological significance of the autophagy observed in cells in which the HCV genome replicates.

MATERIALS AND METHODS

Plasmids. The plasmids pmStrawberry-C1, pmStrawberry-Atg4B^{C74A}, pmRFP-GFP-LC3, pEGFP-LC3, and pEGFP-Atg16L were described previously (7, 8, 24). The plasmids pFGR-JFH1 and pSGR-JFH1 were kind gifts from T. Wakita.

Cell culture. All cell lines were cultured at 37°C under a humidified atmosphere with 5% CO_2. Huh7 cells were cultivated in Dulbecco's modified Eagle's medium (DMEM) supplemented with 10% fetal bovine serum (FBS), nonessential amino acids, 100 U/ml penicillin, and 100 mg/ml streptomycin. For the starvation, the cells were cultivated with Earle's balanced salt solution (EBSS) (Sigma) for 6 h. HCV replicon cells were established as described previously (53). The plasmid pairs pFK-I$_{389}$ neo/NS3-3′/NK5.1 and pFK-I$_{389}$ neo/FGR/NK5.1 and pFGR-JFH1 and pSGR-JFH1 were linearized with ScaI or XbaI. The plasmids pFGR-JFH1 and pSGR-JFH1 were treated with mung bean exonuclease. The linearized DNA was transcribed *in vitro* by using the MEGAscript T7 kit (Applied Biosystems) according to the manufacturer's protocol. The transcribed RNA was electroporated into cells under conditions of 270 V and 960 mF using a Gene Pulser (Bio-Rad). All HCV replicon cells were maintained in DMEM containing 10% FBS, nonessential amino acids, and 1 mg/ml G418 (Nacalai).

Reagents and antibodies. Concanamycin A and bafilomycin A1 were purchased from Sigma and Fluka, respectively. E64D and pepstatin A were from Peptide Institute Inc. Rabbit anti-HCV NS5A polyclonal antibody was described previously (45). Mouse monoclonal anti-JEV NS3 antibody was prepared by immunization using the recombinant protein spanning amino acid residues 171 to 619 of JEV NS3. Rabbit polyclonal anti-LC3 (PM036), mouse monoclonal anti-RFP (8D6), and anti-62/SQSTM1 (5F2) antibodies were purchased from Medical & Biological Laboratories. Rabbit polyclonal anti-cathepsin B (FL-339) and mouse monoclonal anti-LAMP1 (H4A3) antibodies were from Santa Cruz Biotechnology. Mouse monoclonal anti-HCV NS5A (HCM-131-5), rabbit polyclonal anti-β-actin, and mouse monoclonal anti-Golgin97 (CDF4) antibodies were from Austral Biologicals, Sigma, and Invitrogen, respectively. Mouse monoclonal and rabbit polyclonal anti-cathepsin B antibodies were from Calbiochem. Mouse monoclonal anti-p62/SQSTM1 (5F2) and anti-ATP6V0D1 (ab56441) antibodies were from Abcam. Rabbit polyclonal anti-Atg4B antibody was from Sigma. Mouse anti-double-stranded RNA (dsRNA) IgG2a (J2 and K1) antibodies were from Biocenter Ltd. (Szirak, Hungary).

Transfection, infection, and immunoblotting. Transfection and infection were carried out as described previously (53). Each lysosome-enriched fraction was isolated by using the Lysosome Enrichment Kit for Tissue and Cultured Cells (Pierce) according to the manufacturer's protocol. Samples were subjected to 12.5% sodium dodecyl sulfate-polyacrylamide gel electrophoresis. The proteins were transferred to polyvinylidene difluoride membranes (Millipore) and were reacted with the appropriate antibodies. The immune complexes were visualized with Super Signal West Femto substrate (Pierce) and detected by an LAS-3000 image analyzer system (Fujifilm). The protein bands of LC3 and β-actin were quantified by Multi Gauge software (Fujifilm), and the values of LC3 were normalized to those of β-actin.

Fluorescence microscopy. Cells were cultured on glass slides and then fixed with 4% paraformaldehyde in phosphate-buffered saline (PBS) at room temperature for 30 min. After being washed twice with PBS, the cells were permeabilized at room temperature for 20 min with PBS containing 0.25% saponin and then blocked with PBS containing 0.2% gelatin (gelatin-PBS) for 60 min at room temperature. The cells were incubated with gelatin-PBS containing appropriate antibodies at 37°C for 60 min and washed three times with PBS containing 1% Tween 20 (PBST). The resulting cells were incubated with gelatin-PBS containing corresponding fluorescent-conjugated secondary antibodies at 37°C for 60 min and then washed three times with PBST. The stained cells were covered with Vectashield mounting medium containing DAPI (4′,6-diamidino-2-phenylindole) (Vector Laboratories Inc.) and observed with a FluoView FV1000 laser scanning confocal microscope (Olympus). Time-lapse video microscopy was performed at 37°C with a DeltaVision microscope system (Applied Precision Inc.) equipped with a ΔTC3 culture dish system (Bioptechs) for temperature control.

Quantification of pro-cathepsin B. Each cell line was seeded on 12-well type I collagen-coated dishes (IWAKI) and cultured for 48 h. The supernatant and the cells were harvested and subjected to quantification of pro-cathepsin B by using Quantikine human pro-cathepsin B immunoassay (R&D Systems) according to the manufacturer's protocol.

Statistical analysis. Estimated values were represented as the means ± standard deviations. The significance of differences in the means was determined by Student's *t* test.

RESULTS

Autophagy is induced in the HCV replicating cell in a strain-dependent manner. To determine whether autophagy is induced during the replication of HCV, we investigated the phosphoethanolamine (PE) conjugation of LC3 in HCV replicon cells in which HCV RNA was autonomously replicating. As shown in Fig. 1A, the amounts of PE-conjugated LC-3 (LC3-II), a conventional marker for an autophagosomal membrane, in Huh7 cells were slightly increased by starvation, in conjunction with a reduction of the unmodified LC-3 (LC3-I). In contrast, the amount of LC3-II was significantly increased in the subgenomic and full genomic HCV replicon cells of the genotype lb strain Con1 (SGR^{Con1} and FGR^{Con1}), whereas a small amount of LC3-II was detected in the full genomic replicon cells of the genotype 2a strain JFH1 (FGR^{JFH1}). We also examined the subcellular localization of LC3 by using confocal microscopy. Although LC3 was diffusely detected in the cytoplasm of naïve Huh7 cells, small foci of the accumulated LC3 appeared after starvation (Fig. 1B), whereas many LC3 foci that were larger in size than those in the starved cells appeared in the cytoplasm, particularly near the nucleus, in both SGR^{Con1} and FGR^{Con1} cells. However, a low level of LC3 focus formation comparable to that in the starved cells was observed in the FGR^{JFH1} cells. Most of the LC3 foci were not colocalized with NS5A, an HCV protein of the viral replication complex, in the HCV replicon cells, as reported previously (49). Elimination of HCV RNA from the SGR^{Con1} cells by treatment with alpha interferon (SGR^{cured}) abrogated the lipidation and accumulation of LC3 (Fig. 1C and D). Interestingly, overexpression of the HCV polyprotein of genotype 1b by an expression plasmid induced no autophagy (data not shown), suggesting that replication of viral RNA is required for induction of autophagy. Furthermore, neither lipidation nor accumulation of LC3 was observed in SGR^{JEV} cells harboring subgenomic replicon RNA cells of Japanese encephalitis virus (JEV), which is also a member of the family *Flaviviridae* (Fig. 1C and D). These results suggest that replication of HCV but not that of JEV induces autophagy.

The autophagy flux is impaired in the replicon cells of HCV strain Con1 after a step of autophagosome formation. To further examine the autophagy induced in the HCV replicon cells in more detail, Huh7 and SGR^{Con1} cells were treated with pepstatin A and E64D, inhibitors of aspartic protease and cysteine protease, respectively. In this assay, treatment of intact cells capable of inducing autophagy with the inhibitors increases the amount of LC3-II, whereas no increase is observed in cells impaired in the autophagic degradation. The amount of LC3-II was significantly increased in the naïve Huh7

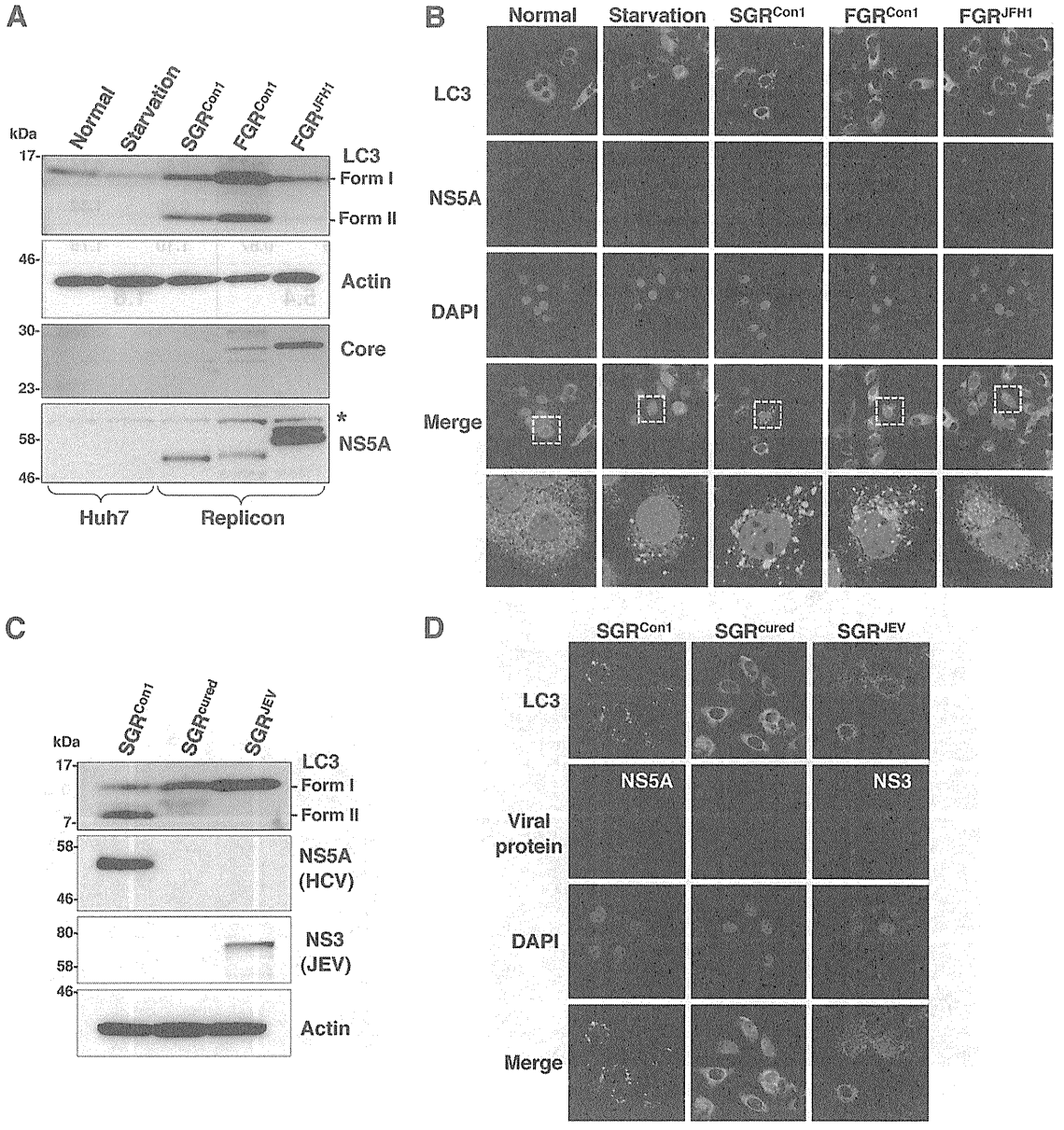

FIG. 1. Induction of autophagy in the HCV replicon cells. (A) The starved Huh7 cells and HCV replicon cells harboring a sub- or full genomic RNA of strain Con1 or strain JFH1 were subjected to immunoblotting using the appropriate antibodies. The asterisk indicates a nonspecific band. (B) Subcellular localizations of LC3 and NS5A were determined by confocal microscopy. The replicon cells and the starved Huh7 cells were stained with DAPI and then reacted with rabbit polyclonal anti-LC3 and mouse monoclonal anti-NS5A antibodies, respectively, followed by Alexa Fluor 488- and 594-conjugated secondary antibodies, respectively. The boxed areas in the merged images are magnified. (C) SGR^{Con1} cells were treated with alpha interferon for 1 week to remove the HCV replicon RNA. The resulting cells were designated SGR^{cured} cells. The SGR^{Con1}, SGR^{cured}, and SGR^{JEV} cells were lysed and subjected to immunoblotting using the appropriate antibodies. (D) Subcellular localization of LC3 and JEV NS3 and HCV NS5A was determined by confocal microscopy after staining with DAPI, followed by staining with rabbit polyclonal anti-LC3 and anti-JEV NS3 antibodies and mouse monoclonal anti-NS5A antibodies and then with the appropriate secondary antibodies. The data shown are representative of three independent experiments.

cells by treatment with the inhibitors, whereas only a slight increase was observed in the SGR^{Con1} cells (5.4-fold versus 1.6-fold) (Fig. 2A), suggesting that autophagy is suppressed in the HCV replicon cells. Furthermore, cytoplasmic accumulation of LC3 was significantly increased in the naïve Huh7 cells by treatment with the inhibitors, in contrast to the only slight increase induced by treatment in the SGR^{Con1} cells (Fig. 2B). In SGR^{Con1} cells, the LC3 foci were colocalized with the polyubiquitin-binding protein p62/SQSTM1, a specific substrate for autophagy (18), suggesting that most of the autophagosomes were distributed in the cytoplasm of the SGR^{Con1} cells (Fig. 2B and C). Next, to examine the autophagy flux in the SGR^{Con1} cells, we monitored the green fluorescent protein (GFP)-conjugated LC3 dynamics in living cells by using time-lapse imaging techniques (see movies in the supplemental material). A large number of small GFP-LC3 foci were detected in the

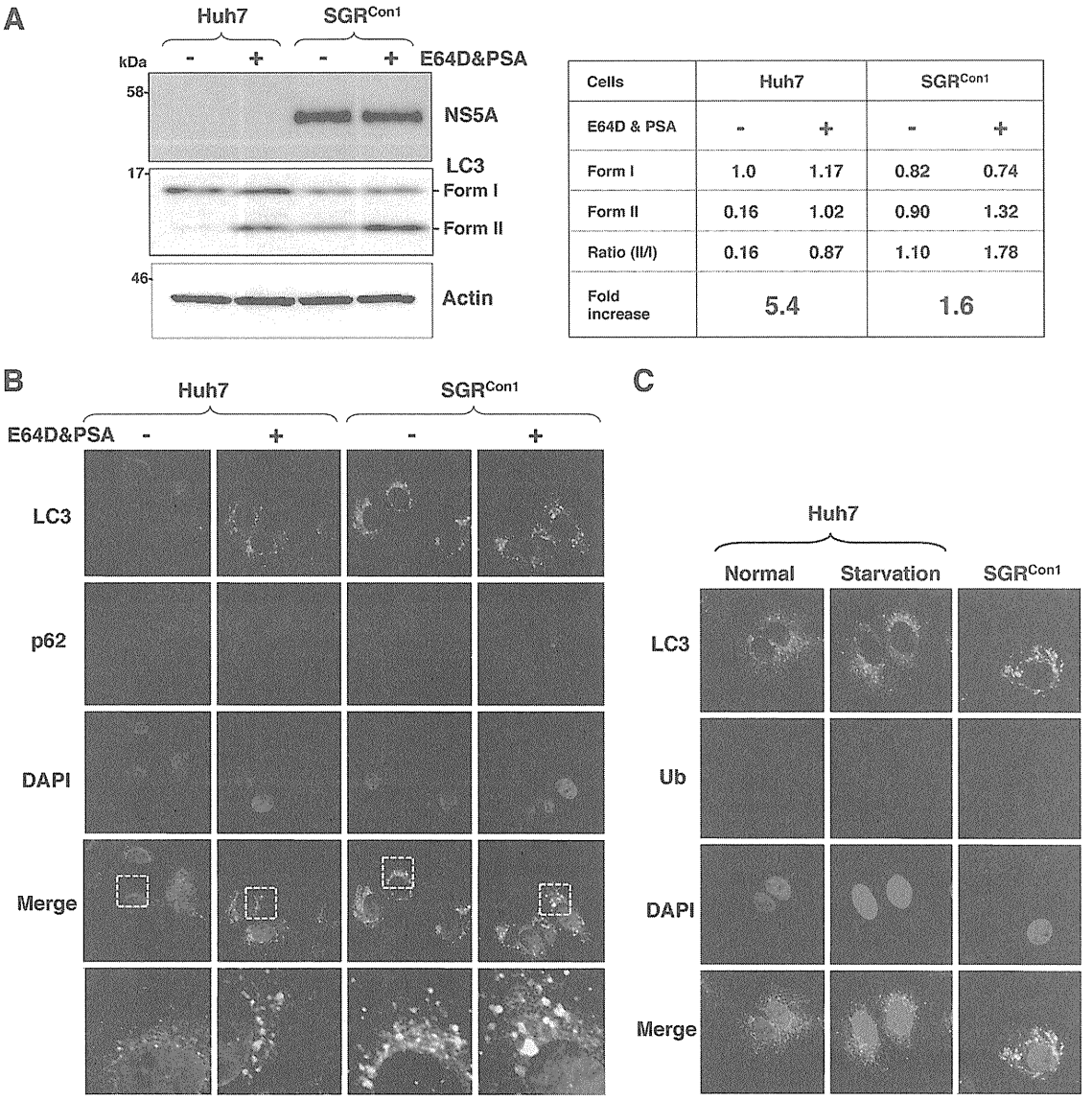

Cells	Huh7		SGR^{Con1}	
E64D & PSA	-	+	-	+
Form I	1.0	1.17	0.82	0.74
Form II	0.16	1.02	0.90	1.32
Ratio (II/I)	0.16	0.87	1.10	1.78
Fold increase	5.4		1.6	

FIG. 2. Autophagy flux is impaired in the HCV replicon cells. Autophagy flux assay using lysosomal protease inhibitors. (A) Huh7 and SGR^{Con1} cells were treated with 20 μM E64D and pepstatin A (PSA) for 6 h, and the cell lysates were subjected to immunoblotting. The density of the protein band was estimated by Multi Gauge version 2.2 (Fujifilm). (B) After nuclear staining with DAPI, the intracellular localizations of LC3 and p62 in each cell were determined by staining with rabbit polyclonal anti-LC3 and mouse monoclonal anti-62 antibodies, respectively, followed by staining with Alexa Fluor 488- and 594-conjugated secondary antibodies, respectively. The resulting cells were observed by confocal microscopy. (C) Colocalization of accumulated LC3 with ubiquitinated proteins (Ub) in SGR^{Con1} cells. Nontreated and starved Huh7 cells and SGR^{Con1} cells were fixed and stained with DAPI and rabbit anti-LC3 and anti-ubiquitin (6C1.17) (BD) polyclonal antibodies, respectively, and then with the appropriate secondary antibodies. Subcellular localizations of LC3 and Ub were determined by confocal microscopy. The data shown are representative of three independent experiments.

starved Huh7 cell, moved quickly, and finally disappeared within 30 min. Although small foci of GFP-LC3 exhibited characteristics similar to those in the starved cells, some large foci exhibited confined movement and maintained constant fluorescence for at least 3 h in the SGR^{Con1} cells. The GFP-LC3 foci in the SGR^{JFH1} cells showed characteristics similar to those in the starved cells. These results support the notion that autophagy flux is suppressed in the SGR^{Con1} cells at some step after autophagosome formation.

Impairment of autolysosomal acidification causes incomplete autophagy in the replicon cell of strain Con1. Recent studies have shown that some viruses inhibit the autophagy pathway by blocking the autolysosome formation (10, 42). Therefore, we determined the autolysosome formation in the HCV replicon cells through the fusion of autophagosome with lysosome. Colocalization of small foci of LC3 with LAMP1, a lysosome marker, was observed in the starved Huh7 cells, SGR^{Con1} cells, and SGR^{JFH1} cells but not in the SGR^{cured} cells (Fig. 3A), suggesting that autolysosomes are formed in the HCV replicon cells of both Con1 and JFH1 strains. The autolysosome is acidified by the vacuolar-type H^+ ATPase (V-ATPase) and degrades substrates by the lysosomal acidic hy-